CCFE-PR(15)59

Guoliang Xia, Yueqiang Liu, Yue Liu, G. Z. Hao, and Li Li

Stabilization of resistive wall mode in tokamaks by drift kinetic effects combined with magnetic feedback

Stabilization of resistive wall mode in tokamaks by drift kinetic effects combined with magnetic feedback

Guoliang Xia[1], Yueqiang Liu[2,3], Yue Liu[1], G. Z. Hao[3], Li Li[4]

[1] ***Key Laboratory of Materials Modification by Laser, Ion and Electron Beams, Ministry of Education, School of Physics and Optoelectronic Technology, Dalian University of Technology, Dalian 116024, People's Republic of China***

[2] ***CCFE, Culham Science Centre, Abingdon, OX14 3DB, UK***

[3] ***Southwestern Institute of Physics, PO Box 432, Chengdu 610041, People's Republic of China***

[4] ***College of Science, Donghua University, Shanghai 201620, People's Republic of China***

Stabilization of resistive wall modes in tokamaks by drift kinetic effects combined with magnetic feedback

Guoliang Xia[1], Yueqiang Liu[2,3,*], Yue Liu[1,*], G. Z. Hao[3], Li Li[4]

[1] Key Laboratory of Materials Modification by Laser, Ion and Electron Beams, Ministry of Education, School of Physics and Optoelectronic Technology, Dalian University of Technology, Dalian 116024, People's Republic of China

[2] CCFE, Culham Science Centre, Abingdon, OX14 3DB, UK

[3]Southwestern Institute of Physics, PO Box 432, Chengdu 610041, People's Republic of China

[4]College of Science, Donghua University, Shanghai 201620, People's Republic of China

[*]E-mails of corresponding authors: Yueqiang.Liu@ccfe.ac.uk; liuyue@dlut.edu.cn

Abstract

The synergetic effects of drift kinetic resonances, the resistive layer dissipation, the magnetic feedback, and the toroidal plasma flow on the stability of the resistive wall mode are numerically investigated using a full toroidal resistive magnetohydrodynamic-kinetic hybrid stability code MARS-K (Liu Y Q *et al* 2008 Phys. Plasmas **15** 112503). It is found that the plasma resistivity, coupled with the favourable average curvature effect, can enlarge the stable domain predicted by the drift kinetic model. A synergy between the precessional drift resonance damping, the magnetic feedback and the plasma flow helps open two stability windows. The width of the inner stability window increases with the feedback gain, but decreases with the flow speed. In addition, optimization of the toroidal phase difference of the feedback gains between the upper and lower active coils can lead to a full suppression of the mode.

(Some figures in this article are in colour only in the electronic version)

1. Introduction

The onset of the resistive wall mode (RWM) has been a major concern for advanced tokamaks [1] such as ITER [2]. The RWM can be viewed as a residual instability from the external ideal kink (XK) mode, which is a global magnetohydrodynamic (MHD) instability driven by plasma current gradient or pressure. The RWM can pose severe operational limits on the achievable beta values of tokamaks and on the discharge duration in RFP devices. In order to maximize the benefit of the concept of advanced tokamaks, which aim at high pressure, large bootstrap current fraction, long pulse or even steady state operation, stabilization of the RWM is a critical issue.

Two approaches are well established to stabilize the mode in tokamaks, namely feedback control using magnetic coils [3-12] or passive stabilization based on toroidal plasma flow damping [13-18]. While significant progress has been made in understanding the feedback control of the RWM in both theory and experiments, including impressive results obtained on RFP devices [19, 20], understanding of the passive stabilization physics is still incomplete, in particular, in view of the recently discovered drift kinetic physics associated with the RWM damping. The experiments from DIII-D [21] and JT-60U [22] showed a very small threshold value of toroidal flow speed, about 0.3% of the Alfven speed, for the complete suppression of the RWM. This value is much lower than that observed from previous magnetic braking experiments with large momentum input. Theoretical models based on magnetic drift kinetic resonances [23-29] seem to provide a reasonable explanation of these new experimental results.

Most theoretical work, with very few exceptions [30-33], uses ideal MHD theory to study the RWM. The role of the plasma resistivity on the RWM stability, in conjunction with the drift kinetic effects from energetic particles, was first analyzed in a recent analytic work [34], where a strong damping of the mode due to the resistive layer dissipation associated with the Glasser-Greene-Johnson effect [35], was demonstrated. Toroidal computation of the resistivity induced RWM damping has been carried out in our recent work [36], but in the context of a fluid model for the RWM. Within the fluid approximation, Ref. 36 also investigated the synergetic effects between the active and passive stabilization of the mode.

This work expands that of Ref. 36, by considering combined effects of several important physics, namely the drift kinetic damping, the magnetic feedback, the resistive layer effects, and the toroidal flow damping, on the stability of the RWM. We consider the same toroidal tokamak model as in Ref. 36, and carry out computational study using the MARS-K code [37]. For the drift kinetic effects, we focus on the precessional drift resonance between with the mode and the trapped thermal ions and electrons.

The multi-physics nature of the problem dictates that we have to explore the mode stability in multi-dimensional space. The parameters that we vary include: the plasma pressure, the on-axis plasma toroidal rotation frequency Ω_0 (with a fixed rotation profile), normalized by the Alfven frequency $\Omega_A = B_0 \Big/ \left(R_0 \sqrt{\mu_0 \rho_0} \right)$, the normalized radial distance d/a of the resistive wall, the plasma resistivity η, normalized by $\eta_0 = \mu_0 R_0^2 \varepsilon^2 \Omega_A$ ($\varepsilon = a/R_0$), the amplitude $|G|$ (normalized by

$G_0 = R_0/\mu_0$) and phase arg(G) of the feedback gain G. Here B_0 is the toroidal vacuum magnetic field at the magnetic axis of the plasma equilibrium, ρ_0 is the on-axis plasma mass density, a the plasma minor radius and R_0 the major radius of the torus, μ_0 is the vacuum magnetic permeability.

The next section describes computational models used in MARS-K. Section 3 specifies a toroidal equilibrium used in this study. Section 4 reports numerical results. Section 5 draws conclusions. A simple analytic model is proposed in Appendix A, in order to qualitatively explain the computational results related to the drift kinetic damping. An analytic model, based on the extended energy principle, including contributions from the perturbed fluid potential energy, the vacuum and the resistive wall energy perturbation, as well as the energy associated with the feedback coils, is derived in Appendix B, in order to demonstrate the synergistic effects between the magnetic feedback and the drift kinetic damping. Finally, Appendix C offers an analytic model for investigating the coil phasing effect in the presence of multiple rows of active control coils.

2. Computational models

Each of the physics models (the single fluid, the resistive plasma, the toroidal flow, the magnetic feedback, the drift kinetic formulation), that we shall employ in this work, has previously been reported in separate publications. For the completeness of discussions, we present below a brief overview of all these physics effects, as well as basic numerical aspects associated with the MARS-K code.

The core part of our formulation is the toroidal hybrid MHD-kinetic model, that combines the single-fluid MHD equations with a self-consistent drift kinetic closure for the perturbed pressure. The eventual fluid and kinetic equations, in the plasma region, are solved together with equations for the resistive wall(s), the active coils, as well as the vacuum itself in the vacuum region.

2.1. The MHD-kinetic hybrid model in MARS-K with plasma flow

The core equations in the plasma region, where the kinetic terms are involved, are written in the Eulerian frame [37, 38]

$$(\gamma + in\Omega)\boldsymbol{\xi} = \mathbf{v} + (\boldsymbol{\xi}\cdot\nabla\Omega)R^2\nabla\phi \tag{1}$$

$$\rho(\gamma + in\Omega)\mathbf{v} = -\nabla\cdot\mathbf{p} + \mathbf{j}\times\mathbf{B} + \mathbf{J}\times\mathbf{b} - \rho[2\Omega\hat{\mathbf{Z}}\times\mathbf{v} + (\mathbf{v}\cdot\nabla\Omega)R^2\nabla\phi] - \nabla\cdot\boldsymbol{\Pi} \tag{2}$$

$$(\gamma + in\Omega)\mathbf{b} = \nabla\times(\mathbf{v}\times\mathbf{B} - \eta\mathbf{j}) + (\mathbf{b}\cdot\nabla\Omega)R^2\nabla\phi \tag{3}$$

$$(\gamma + in\Omega)\, p = -\mathbf{v}\cdot\nabla P \tag{4}$$

$$\mu_0\mathbf{j} = \nabla\times\mathbf{b} \tag{5}$$

where γ is the (complex) eigenvalue of the mode, corrected by a Doppler shift $in\Omega$, with n being the toroidal mode number, Ω the angular frequency of the plasma flow along the toroidal direction ϕ. $(\mathbf{B},\mathbf{J},P)$ are the equilibrium magnetic field, the plasma current density and pressure, respectively. These equilibrium quantities are obtained by the equilibrium code CHEASE [39], which solves the fixed boundary Grad-Shafranov equation. The lower-case quantities $(\boldsymbol{\xi},\mathbf{v},\mathbf{b},\mathbf{j},\mathbf{p})$ represent the plasma displacement, perturbed velocity, magnetic field, current and pressure tensor, respectively. ρ is the unperturbed mass density, R the plasma major radius, $\hat{\mathbf{Z}}$ the unit vector in the vertical direction. $\boldsymbol{\Pi}$ is a viscous stress tensor, chosen in this

work to represent a viscous force damping the parallel sound wave [14], with a numerical coefficient $\kappa_{\|}$ specifying the strength of the damping. η is the plasma resistivity. Note that the fluid compressibility term $5/3P\nabla\cdot\mathbf{v}$ is dropped from Eq. (4) for the perturbed scalar pressure. This term is replaced by the anisotropic part of the full drift kinetic pressure tensors $\mathbf{p}$ [40, 41]

$$\mathbf{p} = p\mathbf{I} + p_{\|}\hat{\mathbf{b}}\hat{\mathbf{b}} + p_{\perp}(\mathbf{I} - \hat{\mathbf{b}}\hat{\mathbf{b}}) \tag{6}$$

where $\mathbf{I}$ is the unit tensor and $\hat{\mathbf{b}} = \mathbf{B}/B$, $B = |\mathbf{B}|$. p is the scalar (isotropic) part of the perturbed pressure, representing the so called adiabatic part of the drift kinetic pressure. Strictly speaking, equation (4) holds only for special equilibrium distribution functions such as Maxwellian, which is what we assume in this work for thermal particles. $p_{\|}(\xi_{\perp})$ and $p_{\perp}(\xi_{\|})$ are the parallel and perpendicular perturbations of the kinetic pressure (the non-adiabatic contribution), computed by

$$p_{\|}e^{-i\omega t+in\phi} = \sum_{e,i}\int d\Gamma M\mathrm{v}_{\|}^2 f_L^1 \tag{7}$$

$$p_{\perp}e^{-i\omega t+in\phi} = \sum_{e,i}\int d\Gamma \frac{1}{2}M\mathrm{v}_{\perp}^2 f_L^1 \tag{8}$$

where an $\exp(-i\omega t + in\phi)$ dependence is explicitly assumed for the perturbation, with the mode (complex) frequency ω. M is the particle mass, $\mathrm{v}_{\|}$ and $\mathrm{v}_{\perp}$ are the parallel and perpendicular (to the equilibrium magnetic field) velocities of particle drift motion. The integral is carried out over the particle velocity space Γ. f_L^1 is the non-adiabatic part of the perturbed particle distribution function, which is derived by solving the perturbed drift kinetic equations for each particle species, the expression for f_L^1 is as follows [37]

$$f_L^1 = -f_\varepsilon^0 \varepsilon_k e^{-i\omega t + in\phi} \sum_{m,l,u} X_m^u H_{ml}^u \lambda_{ml} e^{-in\tilde{\phi}(t) + im\langle\dot{\chi}\rangle t + il\omega_b t} \tag{9}$$

where f_ε^0 is the energy derivative of the particle equilibrium distribution function (which we assumed to be Maxwellian for thermal electrons and ions). ε is the particle total energy, $\varepsilon_k = \varepsilon - Ze\Phi$ is the kinetic energy of the particle, Φ being the equilibrium electrostatic potential with the charge number Z. m is the poloidal Fourier harmonic number. l is the so called bounce harmonic number. $\tilde{\phi}(t) = \phi(t) - \langle\dot{\phi}\rangle t$ denotes the periodic part of the particle motion projected along the toroidal direction, with $\langle\cdot\rangle$ denoting an average over the particle bounce period, ω_b is the particle bounce frequency. Both X_m^u and H_{ml}^u are related to the perturbed particle Largrangian. X_m^u denotes the poloidal Fourier harmonics with respect to the perpendicular fluid displacement and the magnetic field perturbation (the superscript "u" labels these components); H_{ml}^u represents the geometrical factor associated with the particle trajectory in the equilibrium magnetic field. λ_{ml} is the mode-particle resonance operator representing the key drift kinetic physics

$$\lambda_{ml} = \frac{n[\omega_{*N} + (\hat{\varepsilon}_k - 3/2)\omega_{*T} + \omega_E] - \omega}{n\omega_d + [\alpha(m+nq) + l]\omega_b - \omega} \tag{10}$$

where ω_{*N} and ω_{*T} are the diamagnetic drift frequencies due to the density and temperature gradients, respectively. ω_E is the $\mathbf{E}\times\mathbf{B}$ drift frequency due to the equilibrium electrostatic potential. $\hat{\varepsilon}_k = \varepsilon_k / T$ is the particle kinetic energy normalized by temperature T. $\omega_d = \langle\dot{\phi}\rangle$ is the bounce-orbit-averaged toroidal precession drift frequency of particles, including the ω_E drift. ω is the mode complex frequency, with $\gamma = -i\omega$. q is the safety factor. We have neglected the

effect of finite radial excursion width of particles across the magnetic surfaces. $\alpha = 0$ for trapped particles, and $\alpha = 1$ for passing particles. In the latter case ω_b denotes the transit frequency. Although the full MARS-K model includes both bounce/transit and precessional drift resonances, we only consider the magnetic precession drift resonance in this work, assuming that the $\mathbf{E}\times\mathbf{B}$ flow velocity is much below the particle bounce/transit velocity.

As a final remark on the kinetic formulation, we point out that our model is similar to the standard δf -method that has been used in several MHD-kinetic codes and in PIC simulations [42-45]. The major difference is that our drift kinetic assumption, as well as neglecting or approximating the finite orbit width effect (the finite banana width for trapped particles), allows a semi-analytic formulation for the perturbed kinetic pressure tensor, which is then effectively used as the closure for the MHD equations.

2.2. The vacuum and wall models

In the vacuum region, $\mathbf{v}$ and p vanish. The perturbed magnetic field satisfies

$$\begin{aligned} \nabla\times\mathbf{b} &= 0 \\ \nabla\cdot\mathbf{b} &= 0 \end{aligned} \tag{11}$$

The equation for the resistive wall follows a thin shell approximation

$$\gamma b^r = \frac{\eta_w}{\mu_0 h_w}\left(|\nabla r|\Delta\frac{\partial b^r}{\partial r} - \Delta b^\chi \frac{|\nabla r|}{\partial\chi}\right) \tag{12}$$

where η_w and h_w are the resistivity and thickness of the wall, respectively. b^r and b^χ are the contravariant components of the field perturbation, represented in a curvilinear coordinate system (r,χ,ϕ) for a torus

$$\mathbf{b} = b^r \nabla\chi \times \nabla\phi + b^\chi \nabla\phi \times \nabla r + b^\phi \nabla r \times \nabla\chi$$

where r is the radial coordinate, defined as square root of the normalized poloidal magnetic flux (here we use "r" to denote the radial coordinate, in order to avoid confusion of notions to be introduced in the following subsection). χ is the generalized poloidal angle depending on the choice of Jacobian.

2.3. The feedback model

The coil current in the active coils is assumed to be a surface current (similar to the wall eddy current), with the toroidal component of the coil current density represented as δ-functions along the poloidal angle. The poloidal component of the coil current density follows from the divergence-free condition. For a given toroidal mode number n, the toroidal component of the surface current density, for each set of the active coils, can be generally represented as

$$J_\phi^{coil}(r,\chi,\phi) = I_f \delta(r - r_f)\left[\delta(\chi - \chi_U) - \delta(\chi - \chi_L)\right] e^{in\phi}$$

where r_f is the radial location of the active coils; χ_U and χ_L are the upper and lower legs of the window frame coils, respectively; I_f is the total coil current, generally being a complex number. Note that the above expression for the coil current density is valid for a single array of window frame coils along the poloidal angle. With multiple arrays of active coils, extra δ-functions, along the poloidal angle, are added to the expression.

In the numerical implementation, since all the perturbed quantities (including the coil current density) are decomposed in Fourier harmonics along the poloidal angle, the above δ-functions along χ are replaced by narrow Gaussian functions. By

including a sufficiently large number of poloidal Fourier harmonics (from -29 to 29 in this study after a numerical convergence test), the full poloidal spectrum of the window frame coils, that affects the RWM control, is resolved. The above coil current representation has been extensively benchmarked for accuracy in producing the vacuum field, compared with the Biot-Savart law based field computation technique, while MARS-F is applied for modelling the plasma response to resonant magnetic perturbations (RMP) [46, 47].

The equation for the feedback coils depends on the choice of the feedback law. For a negative, proportional feedback, that controls the current I_f in the coils using the magnetic signal $\psi_s(t)$ measured by a set of sensor loops as input, the feedback equation reads [3]

$$M_{sf} I_f = -G\psi_s(t) \tag{13}$$

where G is the dimensionless proportional gain. $\psi_s(t)$ is assumed to be a point-wise poloidal field signal in this work. M_{sf} is the free-space mutual inductance between the feedback coil and the sensor loop, which is a constant for fixed geometrical locations of the feedback and sensor coils. Since this quantity only plays a role of scaling the gain value, we set M_{sf} to be unity in this work.

We also define an open-loop transfer function $P(s)$ [48]

$$P(s) = \frac{\psi_s}{M_{sf} I_f} \tag{14}$$

where s is the Laplace variable representing the mode eigenvalue. It is important to note that the above open-loop transfer function can be computed without directly solving the feedback equation (13). Instead, we can compute $P(s)$ by computing the

plasma response to a given current source flowing in the active coils. In this work, we follow both approaches – the plasma response approach and the direct feedback approach – to study the synergy effect between the kinetic damping and the magnetic feedback on the RWM.

Equations (13) and (14) are combined to yield the closed loop characteristic equation

$$1+GP(s)=0 \tag{15}$$

The solution of the characteristic equation gives the closed-loop eigenvalue s, for a chosen feedback gain G.

2.4. Boundary conditions and numerical aspects

At the plasma-vacuum interface, the boundary condition is equivalent to the conventional perturbed force balance condition for ideal plasma-vacuum interface. This boundary condition is applied to the unperturbed plasma boundary. At the computational boundary (which is assumed to be sufficiently far away), the radial component of the perturbed field is assumed to be zero.

The whole MARS-K formulation can be regarded as a generalized eigenvalue problem, written in a compact form

$$\gamma \mathbf{D}X = \mathbf{A}X\,, \tag{16}$$

where the matrices $\mathbf{D}$ and $\mathbf{A}$ symbolically represent the linearized MHD-kinetic-vacuum operators, with $\mathbf{D}$ essentially associated with inertia. In the pure fluid formulation, the operator $\mathbf{A}$ only depends on equilibrium quantities and does not depend on the mode eigenvalue γ. With the fluid-kinetic hybrid formulation,

however, $\mathbf{A}$ is a strongly non-linear function of γ, via the resonance operator (10). The vector X symbolically represents all the perturbation variables. The solution X is decomposed in Fourier harmonics along the poloidal angle χ and the toroidal angle ϕ

$$X(r,\chi,\phi) = \sum_m \sum_n X_{mn}(r) e^{i(m\chi - n\phi)} \tag{17}$$

For linear perturbations in an axisymmetric torus, the toroidal components decouple from each other. Therefore, we solve for each n-component separately. After the Fourier decomposition along periodic directions, the resulting system of ordinary differential equations along the radial coordinate r is solved using a finite element method [49].

For the pure fluid formulation, the generalized eigenvalue problem (16) is solved using a standard inverse vector iteration scheme [49, 50]. For the hybrid formulation, an extra outer-loop, based on Newton-Raphson iteration scheme, is employed in order to resolve the non-linear dependence of $\mathbf{A}$ on γ.

3. Specification of equilibrium

We consider a toroidal equilibrium, with an up-down symmetric plasma boundary shape as shown in figure 1. This corresponds to a plasma in limiter configuration. The shape of the resistive wall conforms to the plasma boundary surface. We also assume two sets of active coils located just inside the resistive wall, near the top (referred to as “Upper”) and bottom (referred to as “Lower”) of the torus. One set of sensor coils is assumed to be located at the outboard mid-plane, measuring the poloidal magnetic

field at the $\chi = 0$ poloidal angle. We mention that this choice of the geometrical configurations for feedback coils reflects that of several of the present-day tokamak devices such as DIII-D, MAST, ASDEX-Upgrade, KSTAR, EAST.

Figure 2 shows the radial profiles for some key equilibrium quantities. These profiles are either analytically or numerically specified. One of the key features is the slightly reversed magnetic shear in the plasma core, which is often compatible with the advanced tokamak scenario in the presence of an internal transport barrier [51]. The safety factor has the on-axis value of $q_0 = 1.76$, the minimal value of $q_{\min} = 1.60$, and the edge value of $q_e = 3.28$. The normalized beta value is $\beta_N = \beta(\%) a(m) B_0(T) / I_p(MA) = 3.37$, where β is the ratio of the volume averaged plasma pressure to the magnetic pressure, and I_p is the total plasma current. The no-wall beta limit (the stability margin for the $n = 1$ ideal external kink mode without wall) is computed as $\beta_N^{no-wall} = 2.54$, and the beta limit with an ideal wall is $\beta_N^{ideal-wall} = 3.72$. A linear scaling factor for the equilibrium pressure, C_β, is consequently defined as $C_\beta = (\beta_N - \beta_N^{no-wall}) / (\beta_N^{ideal-wall} - \beta_N^{no-wall})$. The radial profile of the safety factor slightly varies as we scan the plasma pressure while keeping $q_{\min}$ fixed. Examples are shown in figure 3. The wall time is assumed to be $\tau_w = \mu_0 h_w r_w / \eta_w = 1.0 \times 10^4 \tau_A$ (r_w is the wall radius, $\tau_A = 1/\Omega_A$ is the Alfven time).

4. Numerical results

In this work, we consider the stabilization of the $n = 1$ RWM. Since we are mostly interested in the mode stability at relatively slow plasma rotation, we only consider

the magnetic precession drift resonance in all the computations. Only kinetic effects from bulk plasma particles are included. A systematic investigation has been carried out in four aspects reported below.

4.1. Precessional drift kinetic effects on the RWM stability

Earlier studies of the RWM stability, relying on the ideal fluid theory [13, 14], predicted that the critical rotation velocity required to fully suppress the mode was a few percent of the Alfven speed. Similar magnitude of critical rotation velocities were also measured in early experiments [52], where an initially fast plasma flow, generated by unbalanced neutral beam momentum injection, was slowed down by subsequent non-linear interaction with either the RWM itself or with external 3D magnetic fields. Recent experiments, with balanced beam injection and hence much slower plasma flow, found much slower critical flow velocity (if at all exists) [21, 22]. These experiments cannot be easily explained by the standard fluid theory, which involves only the sound wave continuum or the shear Alfven wave continuum damping on the mode. This motivates our search for additional mode-particle resonance damping based on the drift kinetic theory.

We mention that different neutral beam injection configurations (unbalanced versus balanced injections) create different hot ion equilibrium distributions, which may also affect the kinetic stabilization of the RWM [53]. This aspect is however beyond the scope of this work. In this study, we shall only consider the drift kinetic effects from thermal particles.

In particular, we are interested in the transition from the fluid prediction to the kinetic prediction. For this purpose, we introduce a numerical parameter α_D in MARS-K, as the fraction factor of the additional kinetic contribution to the RWM damping. Thus $\alpha_D = 0$ recovers the fluid limit, whilst $\alpha_D = 1$ corresponds to the physical fluid-kinetic hybrid result. Figure 4 shows growth rate and mode frequency of the RWM while scanning α_D gradually from 0 to 1, for two choices of on-axis rotation frequency (normalized by the on-axis Alfven frequency) $\Omega_0 = 0.003$ (solid circles) and $\Omega_0 = 0.005$ (solid squares), respectively. Since the plasma rotation is slow, there is little difference in the eigenvalues at the fluid limit. However, at the full fraction of the kinetic contribution ($\alpha_D = 1$), the growth rate of the mode substantially decreases compared to the fluid prediction, as a result of the resonance damping from the precessional drift motion of trapped thermal electrons and ions.

Figures 5(a) and (b) plot the growth rate and the mode frequency, respectively, of the kinetic RWM (i.e. at $\alpha_D = 1$), in the 2D parameter space of on-axis rotation frequency and the equilibrium pressure scaling factor C_β. The plasma central rotation frequency Ω_0 varies between $3.0\times10^{-3}\Omega_A$ and $1.0\times10^{-2}\Omega_A$. A full stabilization of the mode, denoted by black dots in figure 5(a), is achieved. This finding, which is similar to other kinetic studies [54], better explains the recent experimental results. Moreover, if we vary the wall radius as traditionally performed in the fluid study for the RWM [13], we find that decreasing the plasma flow speed enlarges the stable domain, as shown by Fig. 6. A stable window opens by the kinetic damping as the resistive wall moves away from the plasma boundary. Such behavior,

as well as some of other computational results shown below, can be qualitatively explained by a simple analytic model presented in Appendix A. Figure 7 summarizes some of the findings from this analytic model.

The results shown in Fig. 6 are qualitatively similar to the conventional ideal fluid prediction. However, qualitatively new features emerge if we assume a resistive plasma model, as reported below.

4.2. Effects of plasma resistivity on the RWM stability

It has been shown in early analytic work [30-32] that, in the presence of toroidal flow, the plasma resistivity can enhance the passive stabilization of the RWM by the fluid model, compared to the ideal MHD prediction, although the stable window is shown to be narrow (and hence not robust) for a toroidal plasma [33]. The recent analytic work [34], combining the resistive layer damping with the kinetic effects in the presence of toroidal flow, demonstrates a strong damping of the mode due to the coupling to the favourable average curvature stabilization inside the resistive layer. Reference 34 assumes a simple cylindrical geometry and one resistive layer near the plasma boundary, in order to facilitate analytic treatment. Here we numerically investigate the effect of the plasma resistivity on the mode stability, based on full toroidal computations.

We start with the fluid model. The parallel sound wave damping model as described in Sec. 2, with a numerical damping coefficient $\kappa_{\|} = 1.5$, is assumed. Figure 8 compares the growth rates of the fluid RWM with varying plasma pressure

and resistivity. Two cases are compared in figure 8(a) and (b), with vanishing plasma flow, and with a relatively fast flow at $\Omega_0 = 0.03$, respectively. A finite plasma resistivity destabilizes the RWM in the absence of equilibrium flow. This is largely due to the fact that the resistive model poses less constraints on the plasma (the plasma is allowed to reconnect near rational surfaces), therefore the mode is more unstable, although the increase of the mode growth by the plasma resistivity is not substantial – the mode is still primarily driven by the high equilibrium pressure.

The effect of the plasma resistivity is however qualitatively different in the presence of the plasma flow, as shown by figure 8(b). In this case, the growth rate of the mode decreases with increasing the plasma resistivity (i.e. decreasing the Lundquist number S). Again a small quantitative change of the mode growth rate is observed at large S value ($S > 1.0 \times 10^7$). A larger change occurs as the S value is further decreased as shown in figure 9. Here we compute the mode growth rate and frequency in the 2D parameter space Ω_0 and S, while fixing the pressure at $C_\beta = 0.70$. Again the fluid model is used. Again we note the very interesting effect of the plasma resistivity on the mode stability, depending on the flow speed. At slow flow, the plasma resistivity destabilizes the RWM; at fast flow, it stabilizes the mode. The transition from the destabilization to the stabilization occurs at $\Omega_0 \sim 0.015\Omega_A$ in our case. The computed mode frequency also becomes large in this transition region. At sufficiently fast flow, the plasma resistivity changes the stability margin of the RWM. This effect is associated with the Glasser stabilization inside the resistive layer [34]. Similar effect leads to the modification of the stability boundary for the tearing

mode in a toroidal plasma [35].

The general picture remains similar when we add the drift kinetic contributions, as shown in figure 10. The kinetic effects bring in two major changes to the results. (i) The transition region from destabilization to stabilization shifts towards higher rotation frequency. (ii) A (nearly) stable region exists at slow flow and high Lundquist number. This is the consequence of the kinetic drift resonance damping for a plasma that is close to ideal.

4.3. Synergy between magnetic feedback and drift kinetic effects

In an earlier work [36], we investigated the synergetic effect between magnetic feedback and plasma flow on the RWM stabilization, based on a fluid model. We found that the feedback system, combined with plasma rotation, helps open a new stability window. In this work, we study the synergy between feedback and drift kinetic effects, based on the self-consistent MHD-kinetic hybrid model.

Inclusion of kinetic damping again opens two stability windows, as a synergetic effect together with magnetic feedback, as shown by figures 11(a) and (b). In figure 11(a), we fix the plasma rotation at $\Omega_0 = 0.003$ while varying the amplitude of the feedback gain $|G|$, whilst in figure 11(b), we keep the gain amplitude at $|G| = 1.0$ while varying the plasma rotation frequency Ω_0. An ideal plasma model is considered here for the slow flow cases. As shown in Fig. 9, the plasma resistivity does not result in qualitative change of the RWM stability at slow flow. Nevertheless, quantitative investigation of the combined effects of the drift kinetic damping, the

magnetic feedback, as well as the destabilizing effect from the plasma resistivity at slow plasma flow, remains a future work. In both (a) and (b), we choose internal poloidal sensors with vanishing phase for the feedback gain. The plots show that the growth rate of the RWM is reduced, and the width of the new stable window (the inner one) in d/a is increased, either with increase of the feedback gain or decrease of the rotation frequency. The latter occurs at relatively slow flow, where smaller rotation frequency leads to a better resonance with precessional drift of thermal particles. The appearance of this new stability window is mainly due to the feedback stabilization of the RWM, when the wall is closer to the plasma that reduces the mode growth rate. The results shown in Fig. 11 are qualitatively reproduced by the analytic model from Appendix A, with results shown in Fig. 7.

The conventional stability window (the outer one) is narrow for our case, and is not significantly affected by the choice of the feedback gain, as shown by figure 11(a). The variation of the flow speed, on the other hand, substantially modifies the conventional stability window, as shown by figure 11(b). Neither feedback nor rotation has appreciable effect on the stability of the external kink branch (XK).

Figure 11(a) shows that variation of the feedback gain, near the normalized value of 1, mainly affects the width of the new (inner) stability window. This is systematically demonstrated by figure 12, where we plot the marginal stability curve in the $|G|-d/a$ space, at a fixed plasma flow $\Omega_0 = 0.003$. The dashed horizontal line indicates the stability boundary for the XK. As mentioned above, this margin is insensitive to the feedback gain nor the plasma rotation speed. The solid curve

represents the stability margin for the RWM. Note a flat upper boundary (associated with the conventional stability window) at relatively small feedback gain. However, at sufficiently large gain amplitude, the two stable windows merge, resulting in a fully stabilized RWM by both feedback and kinetic damping. The critical value of the feedback gain, for the full stabilization, is about 1.5 in this case.

As already demonstrated in reference 36, there are two approaches for computing the critical amplitude of the feedback gain for the mode stabilization. One is a straightforward approach, by directly tracking the growth rate of the closed loop system, in the presence of drift kinetic effects. The alternative approach (referred to as the Nyquist approach) is to compute the open loop plasma response transfer function $P(s)$, defined by equation (14). Both methods should produce the same results, which is numerically verified by the results shown in figure 13. Here we compare four critical curves in the domain of $|G| - \arg(G)$, for two choices of the wall radius. The plasma flow speed is fixed. Again an ideal plasma assumption is adopted. First of all, the two approaches recover the same critical curves as expected. Secondly, we find that negative phase of the feedback gain requires less critical gain amplitude. This is because the feedback with negative gain phase (within the reference system as defined in MARS-K) enhances the mode rotation, which follows the direction of the plasma flow, and thus yielding a stronger damping for the RWM.

4.4. Effects of phase difference between upper and lower active coil currents

In our feedback system, we assume that the toroidal phase of the feedback gain can be

independently varied for the upper and lower sets of active coils. Since these two sets share the same sensor signal, the phase difference in the feedback gain is equivalent to that of the coil currents, between the upper and lower sets. Obviously this phase difference can be optimized, in order to obtain the best synergetic performance between feedback and kinetic damping.

We first examine the symmetry issue with the upper and lower coils. Figure 14 shows the closed loop growth rate in the presence of a finite (slow) flow and the drift kinetic effects, where we only turn on one set of the active coils at a time. We find that the two sets of coils do not perform symmetrically for the mode stabilization, assuming the same (zero) phase for the feedback gain. The symmetry is broken by the finite toroidal flow, which induces a finite mode rotation frequency. In our case, the upper coil feedback further enhances the mode rotation, yielding a stronger stabilization of the mode. Similar to earlier results reported in this work, the asymmetry of the coil configuration does not affect the stability of the XK.

Figure 15 shows results where we keep the feedback gain amplitude the same for both sets of coils, but vary the toroidal phase of the feedback gain for these two sets. We note that variation of the feedback gain does modify the stability windows. In this case, the stabilization from the synergetic effects is stronger with a larger phase difference. A more systematic phase scan will be reported in figure 17. Next we examine the effects of the (relative) gain amplitude (between upper and lower coils) on the mode stability, while fixing the phase difference between two coils. The results are reported in figure 16. Two observations can be made here. (i) At fixed gain phase

for both the upper and lower sets of coils, 40° and 20°, respectively, in this case, different gain amplitude changes outer stability window. In particular, a larger gain for the lower set of coils is counter-productive for the mode stabilization in this case. (ii) Keeping the gain phase difference the same (20°) but varying the individual phase values also leads to different stability window. This leads to the conclusion that the optimal gain phase can only be obtained by simultaneous optimization of both gains for the upper and lower coils.

Figure 17 reports results from such a 2D space scan. Here we keep the gain amplitude of the upper and lower coils the same, $|G| = 0.6, 0.6$. The normalized plasma on-axis rotation frequency is also fixed at $\Omega_0 = 0.003$. Both the real and imaginary parts, in figures 17(a) and (b), respectively, are plotted as we vary the toroidal phase for the upper and lower coil gains. The solid curve shows the stability boundary in the $\phi_U - \phi_L$ plane. The area circled by this curve corresponds to the full stabilization of the RWM, and hence represents the optimal choice for the feedback phasing.

The pattern (stabilization versus destabilization depending on the choice of the feedback phasing) shown in figure 17 is inherently related to the toroidal phasing introduced by the active control system, with that by the passive system as a result of the drift kinetic damping. This can be qualitatively understood from a single-pole analytic model, which is presented in Appendix C. The results from this single model are plotted in figure 18, where we choose an open loop unstable RWM, with the growth rate $\gamma_0 = 1.77 \times 10^4$ and the mode frequency $\omega_0 = 2.59 \times 10^4$. The gain

amplitude is again fixed at $|G_U| = |G_L| = 0.6$. The (complex) residuals of the single-pole approximation, representing the mode response to the upper and lower coils, are specified as $|R_U| = 1.75 \times 10^4$, $\hat{\phi}_U = -20^\circ$; $|R_L| = 1.85 \times 10^{-4}$, $\hat{\phi}_L = 100^\circ$, respectively. These choices of fitting parameters produce qualitatively very similar results, as that from directly MARS-K computations (cf. figure 17). Examination of the single-pole model shows that the optimal coil phasing corresponds to the case, when the toroidal phase of the feedback gain cancels that of mode response (i.e. the residual) to the upper and lower coils, respectively. To the lowest order (single-pole) approximation, and assuming the same gain amplitude for upper and lower coils, the optimal coil phasing does not depend on the open-loop mode eigenvalue. In other words, it does not depend on specific passive damping physics of the RWM.

5. Conclusions

We have carried out detailed numerical investigation of the synergetic effect among the drift kinetic effects, the plasma flow, the plasma resistivity, as well as the magnetic feedback on the RWM stabilization, based on a fully toroidal resistive MHD-kinetic, non-perturbative hybrid model.

By gradually increasing the drift kinetic contribution to the passive damping of the RWM, we identify a strong stabilizing role played by the precessional drift resonance effects, in particular at slow or even vanishing plasma flow. The plasma resistivity can also contribute to the passive stabilization, but only at a finite flow. In fact a critical flow speed exists, across which the role of the plasma resistivity

switches from destabilization to stabilization.

The drift kinetic effects from trapped thermal particles, combined with the magnetic feedback and plasma flow, help to open two stability windows as the wall radius changes. The resulting double stability window is shown in various combinations of parameter spaces. Finally, we find that the optimal choice of the toroidal phase of the feedback gain enhances the synergy effect, producing fully stable domain for the RWM.

Acknowledgments

This work is supported by NSFC with Grant No. 11275041, 11405029, 11428512, and NMCSFP with Grant No. 2014GB124004. This work has been carried out within the framework of the EUROfusion Consortium and has received funding from the Euratom research and training programme 2014-2018 under grant agreement No. 633053 and from the RCUK Energy Programme [grant number EP/I501045]. The views and opinions expressed herein do not necessarily reflect those of the European Commission.

Appendix A. A simplified analytic model for the kinetic RWM

Below we show a simplified, zero-dimensional model of the kinetic RWM, which can be used to qualitatively explain the numerical findings report in this work. In the presence of the drift kinetic damping, the dispersion relation for the RWM can be devised based on an extended energy principle,

$$\frac{\delta W_\infty + \gamma\tau_w \delta W_b}{1+\gamma\tau_w} + \delta W_k + (\gamma + i\omega_E)D = 0 \qquad \text{(A.1)}$$

where δW_∞ and δW_b are the perturbed fluid potential energies without wall and with an ideal wall at location b, respectively. The second term δW_k denotes the perturbed drift kinetic energy. The last term in Eq. (A.1) represents additional damping physics (parallel sound wave damping, Alfven or sound wave continuum damping etc.). The key physics effect in the drift kinetic term (the second term) is the mode-particle resonances [55]. Therefore, as a gross simplification, we keep only the resonance operator in δW_k, neglecting the particle energy and pitch angle dependence, as well as all geometrical effects associated with the equilibrium magnetic geometry. This leads to a simple expression for the drift kinetic energy perturbation [23],

$$\delta W_k \sim c\left[\frac{\omega_{*i} + \omega_E - i\gamma}{\omega_{di} + \omega_E - i\gamma} + \frac{\omega_{*e} + \omega_E - i\gamma}{\omega_{de} + \omega_E - i\gamma}\right] \qquad \text{(A.2)}$$

where ω_{*i} and ω_{*e} are the diamagnetic drift frequencies for thermal ions and electrons, respectively. ω_{di} and ω_{de} are the toroidal magnetic precession drift frequencies for these two particle species. ω_E is the $\mathbf{E}\times\mathbf{B}$ drift frequency. The coefficient c can be viewed as a "lumped" factor over all other effects that we have neglected.

For simplicity, we shall consider a case with $\omega_{*i} = -\omega_{*e} = \omega_*$ and $\omega_{di} = -\omega_{de} = \omega_d$. Inserting Eq. (A.2) into (A.1), we obtain a nonlinear dispersion relation for the eigenvalue of the kinetic RWM,

$$\hat{\gamma} = \frac{1 - C(\hat{\gamma})}{\hat{\gamma}_f^{-1} + C(\hat{\gamma})}, \qquad C(\hat{\gamma}) = a\frac{\hat{\omega}_* \hat{\omega}_d + (\hat{\gamma} + i\hat{\omega}_E)^2}{\hat{\omega}_d^2 + (\hat{\gamma} + i\hat{\omega}_E)^2} + (\hat{\gamma} + i\hat{\omega}_E)\hat{D} \tag{A.3}$$

where the mode's eigenvalue, as well as all the other frequencies, is normalized by the wall time τ_w, and $\hat{\gamma}_f = \gamma_f \tau_w = -\delta W_\infty / \delta W_b$, $a = -2c/\delta W_\infty$, $\hat{D} = -D/\tau_w \delta W_\infty$. The dispersion relation (A.3) is a fourth order algebraic equation with respect to the mode's eigenvalue $\hat{\gamma}$. Among the four roots, two are degenerated, at the limit of $a \to 0$, to satisfy the condition of vanishing denominator for the second equation of (A.3). These two roots are therefore introduced mainly by the gross simplification of the drift kinetic integrations in the particle velocity space. Among the remaining two physical roots, one is always stable, representing the so-called plasma mode [13]. The other is the kinetically modified RWM. This branch qualitatively re-produces all the parametric dependences that we find from the full toroidal MARS-K computations. A set of results, obtained using this analytic model, are reported in Fig. 7.

Appendix B. An energy principle for the RWM with drift kinetic damping and magnetic feedback stabilization

In order to demonstrate the synergistic effect between the drift kinetic damping and the active control, below we construct an analytic model based on the perturbed energy principle for the RWM. Unlike the straightforward energy analysis approach employed in [56], here we use a short-cut technique which allows to quickly establish energy principle in the presence of feedback. We first introduce this technique by a simple example without kinetic terms.

Assuming a case of fluid RWM in the presence of feedback, the energy principle, without any additional damping and without the plasma inertia, can generally be written as

$$\delta W_p + \frac{\delta W_\infty^v + \gamma\tau_w \delta W_b^v}{1+\gamma\tau_w} + \delta W_{fb} = 0 \qquad \text{(B.1)}$$

where δW_p is the perturbed fluid potential energy within the plasma, δW_∞^v and δW_b^v are the perturbed vacuum energy without and with an ideal conducting wall, respectively. δW_{fb} is the perturbed energy associated with the feedback system (the control coils). On the other hand, the open loop response of this simple fluid RWM system can be exactly represented by a single pole transfer function

$$P(s) = \frac{R}{s - s_0} \qquad \text{(B.2)}$$

where $s_0 = -\delta W_\infty / \delta W_b$ is the open loop eigenvalue of the RWM. The residual factor R measures the response of the mode to the feedback system. This factor is essentially determined by the feedback coil geometry. The eigenvalue of the closed loop system, with a control gain G, satisfies the following equation

$$1 + GP(s) = 0 \qquad \text{(B.3)}$$

Combining Eqs. (B.2) and (B.3), and comparing the result with Eq. (B.1), we easily find the perturbed energy associated with the feedback system

$$\delta W_{fb} = \frac{GR\delta W_b}{1+s} \qquad \text{(B.4)}$$

where $s = \gamma\tau_w$ is the closed loop eigenvalue of the RWM. Thus Eq. (B.1), together with (B.4), represents the energy principle for the feedback controlled RWM. We note that our approach here is rather different from that of Ref. [56]. The latter was

proposed essentially for the purpose of computational implementation for the toroidal code, without introducing analytically tractable quantities.

The inclusion of the drift kinetic term complicates the derivations. However, if we assume a simple structure for the perturbed drift energy contribution such as $\delta W_k = c_2 \delta W_b / (\omega_d - is)$, which represents the key physics of the drift kinetic resonance (here between the mode and the precessional drifts of a single particle species), the generic energy balance equation

$$\delta W_p + \frac{\delta W_\infty^v + \gamma \tau_w \delta W_b^v}{1 + \gamma \tau_w} + \delta W_k + \delta W_{fb} = 0 \tag{B.5}$$

can be simplified into

$$\frac{-s_0 + s}{1+s} + \frac{c_2}{\omega_d - is} + \frac{\delta W_{fb}}{\delta W_b} = 0 \tag{B.6}$$

Again note that the open-loop RWM response for this case can be exactly represented by a two-pole transfer function (one pole comes from the fluid part, whilst the other comes from the drift kinetic contribution)

$$P(s) = \frac{R_1}{s - s_1} + \frac{R_2}{s - s_2} \tag{B.7}$$

where the two poles satisfy the open loop dispersion relation, i.e. Eq. (B.6) without the feedback contribution

$$\frac{-s_0 + s_{1,2}}{1 + s_{1,2}} + \frac{c_2}{\omega_d - i s_{1,2}} = 0 \tag{B.8}$$

Combining Eqs. (B.3, B.7, B.8), and comparing with Eq. (B.6), we find

$$\delta W_{fb} = iG \delta W_b \frac{R_1 s_2 + R_2 s_1 - (R_1 + R_2) s}{(1+s)(\omega_d - is)} \tag{B.9}$$

Equation (B.5), together with (B.9), thus gives the RWM dispersion relation in the

presence of both the drift kinetic and the feedback contributions. As one particular aspect, it shows the (self-consistent) modification of the drift kinetic resonance by the feedback action.

Appendix C. A single-pole model of the coil phasing for the RWM control

Here with a simple analytic model, we shall try to elucidate important physics associated with the feedback-kinetic synergy study, that is numerically carried out in this work. We assume a single pole model for the mode's response to two sets of active coils. The response is specified by two frequency-dependent transfer functions, for the upper and lower control coils, respectively,

$$P_U(s)=\frac{R_U}{s-s_0},\qquad P_L(s)=\frac{R_L}{s-s_0} \tag{C.1}$$

where $s_0=\gamma_0+i\omega_0$ is the RWM eigenvalue with flow and kinetic effects, but without feedback (open-loop). $s=\gamma+i\omega$ is the closed loop eigenvalue. The (complex) residuals factors $R_U=\left|R_U\right|e^{i\hat{\phi}_U}$ and $R_L=\left|R_L\right|e^{i\hat{\phi}_L}$ characterize the mode's response to the coil currents. Note that generally speaking, s_0 is also a complex number as a result of passive stabilization of the mode by plasma flow, kinetic effects, resistive layer damping, etc.

Assuming that both active coil currents are driven by the same sensor signal, the closed-loop eigenvalue is determined by the solution of the following equation

$$1+G_UP_U(s)+G_LP_L(s)=0 \tag{C.2}$$

where $G_U=\left|G_U\right|e^{i\phi_U}$ and $G_L=\left|G_L\right|e^{i\phi_L}$ are the complex feedback gain. If we further

assume $|G_U| = |G_L| = |G|$, the eigenvalue of the closed-loop system is easily found to be

$$s = s_0 - |G|[|R_U| e^{i(\phi_U + \hat{\phi}_U)} + |R_L| e^{i(\phi_L + \hat{\phi}_L)}] \tag{C.3}$$

which can be re-written for the mode growth/damping rate and the mode frequency separately,

$$\begin{cases} \gamma = \gamma_0 - |G|[|R_U| \cos(\phi_U + \hat{\phi}_U) + |R_L| \cos(\phi_L + \hat{\phi}_L)] \\ \omega = \omega_0 - |G|[|R_U| \sin(\phi_U + \hat{\phi}_U) + |R_L| \sin(\phi_L + \hat{\phi}_L)] \end{cases} \tag{C.4}$$

This shows that the optimal coil phasing, resulting in the strongest damping of the mode, corresponds to the choices of $\phi_U = -\hat{\phi}_U$, $\phi_L = -\hat{\phi}_L$, i.e. when the toroidal phase of the feedback gain cancels that of mode response (the residual) to the upper and lower coils, respectively.

Within the single-pole approximation, and assuming the same gain amplitude for upper and lower coils, the optimal coil phasing does not depend on the open-loop mode eigenvalue. In more realistic cases, a single-pole model is often insufficient [48]. And the coil phasing effects can be more complicated. In general, the stability of the closed-loop will depend on not only on the passive eigenvalue γ_0 and the mode response to the active coil currents, but also on both amplitude and phase of the feedback gain.

References

[1] Chu M S, Okabayashi M 2010 *Plasma Phys. Control. Fusion* **52** 123001

[2] Hender T C *et al* Progress in the ITER Physics Basis, Chapter 3: MHD stability, operation limits and disruptions 2007 *Nucl. Fusion* **47** S128-S202

[3] Liu Y Q, Bondeson A, Fransson C M, Lennartson B, Breitholtz C 2000 *Phys. Plasmas* **7** 3681

[4] Okabayashi M *et al* 2001 *Phys. Plasmas* **8** 2071

[5] Liu Y Q, Bondeson A 2002 *Plasma Phys. Control. Fusion* **44** L21-L28

[6] Chu M S *et al* 2004 *Phys. Plasmas* **11** 2497

[7] Liu Y Q, Bondeson A, Gribov Y, Polevoi A 2004 *Nucl. Fusion* **44** 232-242

[8] Strait E J *et al* 2004 *Phys. Plasmas* **11** 2505

[9] Wang Z R, Guo S C 2011 *Nucl. Fusion* **51** 053004

[10] Li L, Liu Y, Liu Y Q 2012 *Phys. Plasmas* **19** 012502

[11] Fransson C M, Lennartson B, Breitholtz C, Bondeson A, Liu Y Q 2000 *Phys. Plasmas* **7** 4143

[12] Bondeson A, Liu Y Q, Fransson C M, Lennartson B, Breitholtz C, Taylor T S 2001 *Nucl. Fusion* **41** 455

[13] Bondeson A, Ward D 1994 *Phys. Rev. Lett.* **72** 2709

[14] Chu M S, Greene J M, Jensen T H, Miller R L, Bondeson A, Johnson R W, Mauel M E 1995 *Phys. Plasmas* **2** 2236

[15] Betti R, Freidberg J P 1995 *Phys. Rev. Lett.* **74** 2949

[16] Strait E J, Taylor T, Turnbull A, Ferron J, Lao L, Rice B, Sauter O, Thompson S, Wróblewski D 1995 *Phys. Rev. Lett.* **74** 2483

[17] Gregoratto D, Bondeson A, Chu M S, Garofalo A M 2001 *Plasma Phys. Control. Fusion* **43** 1425-1439

[18] Gimblett C G, Hastie R J, Van der Linden R A M, Wesson J A 1996 *Phys. Plasmas* **3** 3619

[19] Drake J R *et al* 2005 *Nucl. Fusion* **45** 557-564

[20] Martin P *et al* 2009 *Nucl. Fusion* **49** 104019

[21] Reimerdes H *et al* 2007 *Phys. Rev. Lett.* **98** 055001

[22] Takechi M, Matsunaga G, Aiba N, Fujita T, Ozeki T, Koide Y, Sakamoto Y, Kurita G, Isayama A, Kamada Y 2007 *Phys. Rev. Lett.* **98** 055002

[23] Liu Y Q *et al* 2009 *Phys. Plasmas* **16** 056113

[24] Liu Y Q *et al* 2010 *Plasma Phys. Control. Fusion* **52** 104002

[25] Hu B, Betti R 2004 *Phys. Rev. Lett.* **93** 105002

[26] Liu Y Q, Chu M S, Gimblett C G, Hastie R J 2008 *Phys. Plasmas* **15** 092505

[27] Berkery J W, Sabbagh S A, Reimerdes H, Betti R, Hu B, Bell R E, Gerhardt S P, Manickam J, Podestà M 2010 *Phys. Plasmas* **17** 082504

[28] Chapman I T, Gimblett C G, Gryaznevich M P, Hender T C, Howell D F, Liu Y Q, Pinches S D 2009 *Plasma Phys. Control. Fusion* **51** 055015

[29] Hao G Z, Wang A K, Liu Y Q, Qiu X M 2011 *Phys. Rev. Lett.* **107** 015001

[30] Finn J M 1995 *Phys. Plasmas* **2** 3782

[31] Bondeson A, Xie H X 1997 *Phys. Plasmas* **4** 2081

[32] Betti R 1998 *Phys. Plasmas* **5** 3615

[33] Bondeson A, Gimblett C G, Hastie R J 1999 *Phys. Plasmas* **6** 637

[34] He Y, Liu Y Q, Liu Y, Hao G, Wang A 2014 *Phys. Rev. Lett.* **113** 175001

[35] Glasser A H, Greene J M, Johnson J L 1975 *Phys. Fluids* **18** 875
[36] Xia G, Liu Y, Liu Y Q 2014 *Plasma Phys. Control. Fusion* **56** 095009
[37] Liu Y Q, Chu M S, Chapman I T, Hender T C 2008 *Phys. Plasmas* **15** 112503
[38] Wang Z R, Guo S C, Liu Y Q, Chu M S 2012 *Nucl. Fusion* **52** 063001
[39] Lütjens H, Bondeson A, Sauter O 1996 *Comput. Phys. Commun.* **97** 219
[40] Antonsen T M, Lee Y C 1982 *Phys. Fluids* **25** 132
[41] Porcelli F, Stankiewicz R, Kerner W, Berk H L 1994 *Phys. Plasmas* **1** 470
[42] Glasser A H, Sovinec C R, Nebel R A, Gianakon T A, Plimpton S J, Chu M S, Schnack D D, Team t N 1999 *Plasma Phys. Control. Fusion* **41** A747
[43] Kim C C, Sovinec C R, Parker S E 2004 *Comput. Phys. Commun.* **164** 448-455
[44] Jolliet S, Bottino A, Angelino P, Hatzky R, Tran T M, McMillan B F, Sauter O, Appert K, Idomura Y, Villard L 2007 *Comput. Phys. Commun.* **177** 409-425
[45] Pinches S D *et al* 1998 *Comput. Phys. Commun.* **111** 133-149
[46] Liu Y Q, Kirk A, Gribov Y, Gryaznevich M P, Hender T C, Nardon E 2011 *Nucl. Fusion* **51** 083002
[47] Liu Y Q, Kirk A, Sun Y, Cahyna P, Chapman I T, Denner P, Fishpool G, Garofalo A M, Harrison J R, Nardon E 2012 *Plasma Phys. Control. Fusion* **54** 124013
[48] Liu Y Q 2007 *Comput. Phys. Commun.* **176** 161-169
[49] Bondeson A, Vlad G, Lütjens H 1992 *Phys. Fluids B* **4** 1889
[50] Liu D H, Bondeson A 1999 *Comput. Phys. Commun.* **116** 55-64
[51] Bondeson A, Liu D-H, Söldner F, Persson M, Baranov Y F, Huysmans G 1999 *Nucl. Fusion* **39** 1523
[52] Haye R J L, Bondeson A, Chu M S, Garofalo A M, Liu Y Q, Navratil G A, Okabayashi M, Reimerdes H, Strait E J 2004 *Nucl. Fusion* **44** 1197-1203
[53] Liu Y Q, Chapman I T, Graves J P, Hao G Z, Wang Z R, Menard J E, Okabayashi M, Strait E J, Turnbull A 2014 *Phys. Plasmas* **21** 056105
[54] Liu Y Q, Chu M S, Chapman I T, Hender T C 2009 *Nucl. Fusion* **49** 035004
[55] Liu Y Q, Albanese R, Portone A, Rubinacci G, Villone F 2008 *Phys. Plasmas* **15** 072516
[56] Chu M S, Chance M S, Glasser A H, Okabayashi M 2003 *Nucl. Fusion* **43** 441-454

Figure caption:

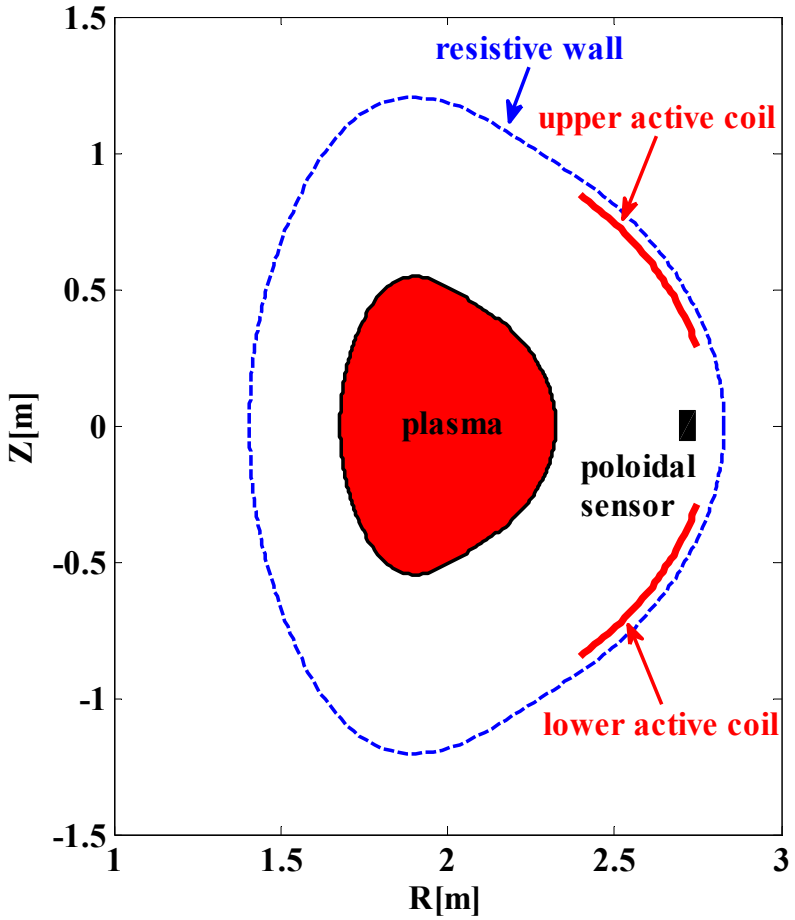

Figure 1. Geometry of a toroidal equilibrium with up-down symmetric plasma boundary shape, a resistive wall conformal to the plasma boundary, two sets of active coils and one set of poloidal sensor coils located just inside the wall.

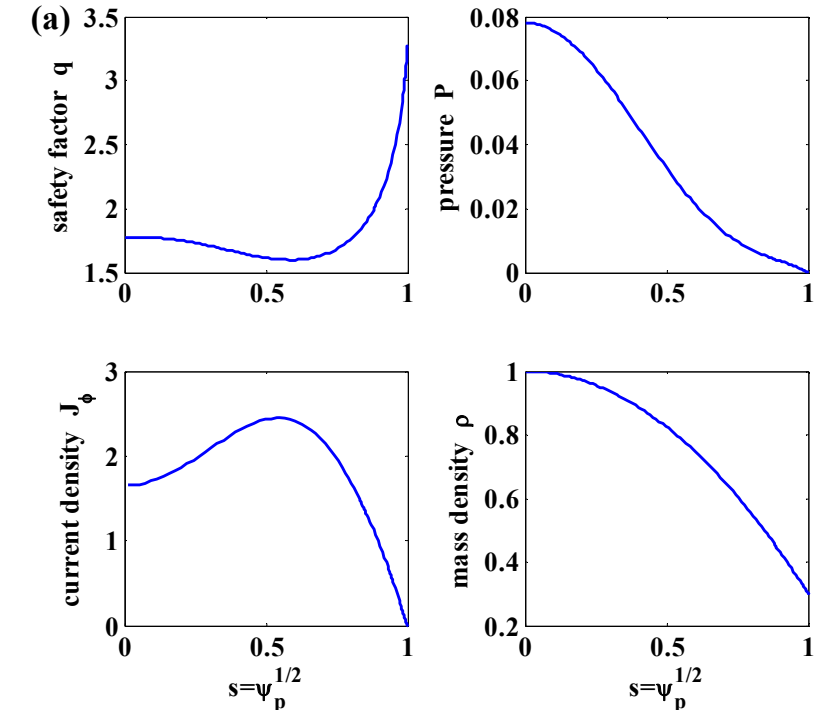

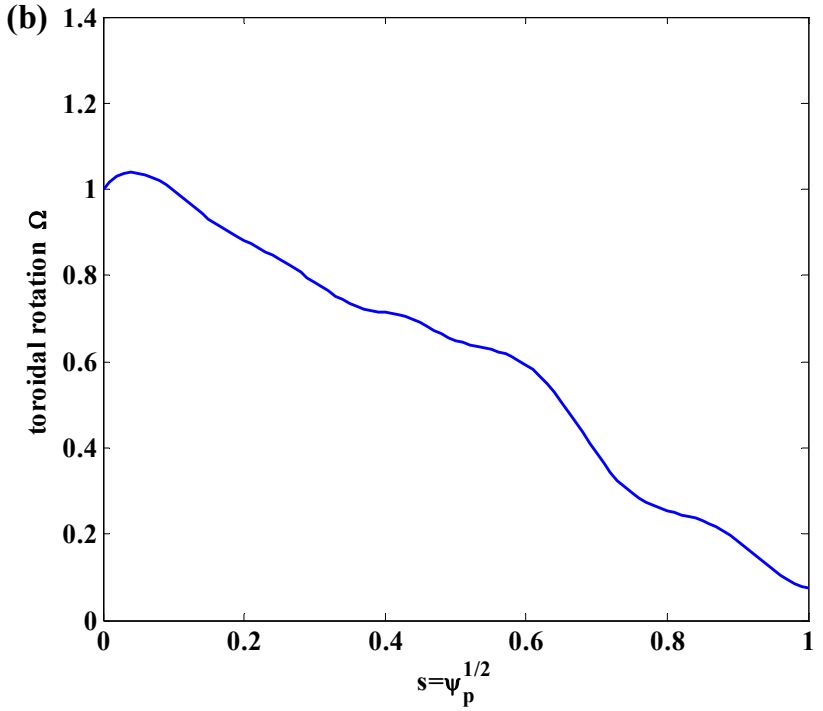

Figure 2. (a) Equilibrium profiles for the safety factor q, the plasma pressure P normalized by B_0^2/μ_0, the toroidal current density J_ϕ normalized by $B_0/(\mu_0 R_0)$ and the plasma mass density ρ normalized to unity at the magnetic axis. (b) The

radial profile of the angular frequency for the plasma toroidal rotation, normalized to unity at the magnetic axis. Here ψ_p is the normalized equilibrium poloidal flux.

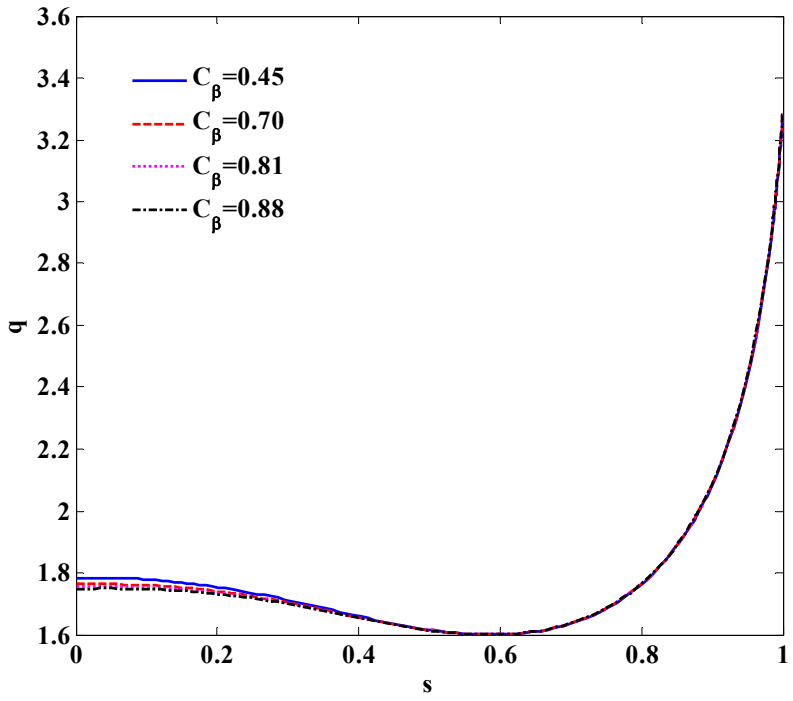

Figure 3. Radial profiles of the safety factor q with varying plasma pressure scaling factor C_β. The minimal q value is fixed 1.6.

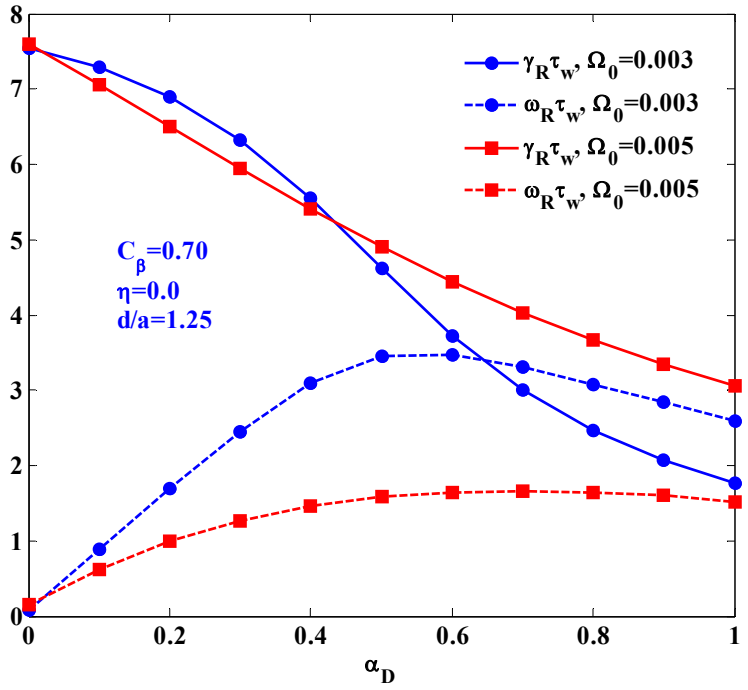

Figure 4. Growth rate (solid lines) and mode frequency (dashed lines) of the RWM versus the kinetic scaling factor α_D, for different plasma rotation frequencies, $\Omega_0 = 0.003$ (solid circles) and $\Omega_0 = 0.005$ (solid squares), respectively. Factor α_D denotes the fraction of the kinetic contribution to the total potential energy, such that $\alpha_D = 0$ corresponds to the case of fluid RWM, whilst $\alpha_D = 1$ corresponds to the full kinetic RWM. The other parameters are $C_\beta = 0.70$, $\eta = 0.0$, $\kappa_{\|} = 0.0$ and $d/a = 1.25$. The on-axis rotation frequency Ω_0 is normalized by the Alfven frequency Ω_A. No feedback is included in these computations.

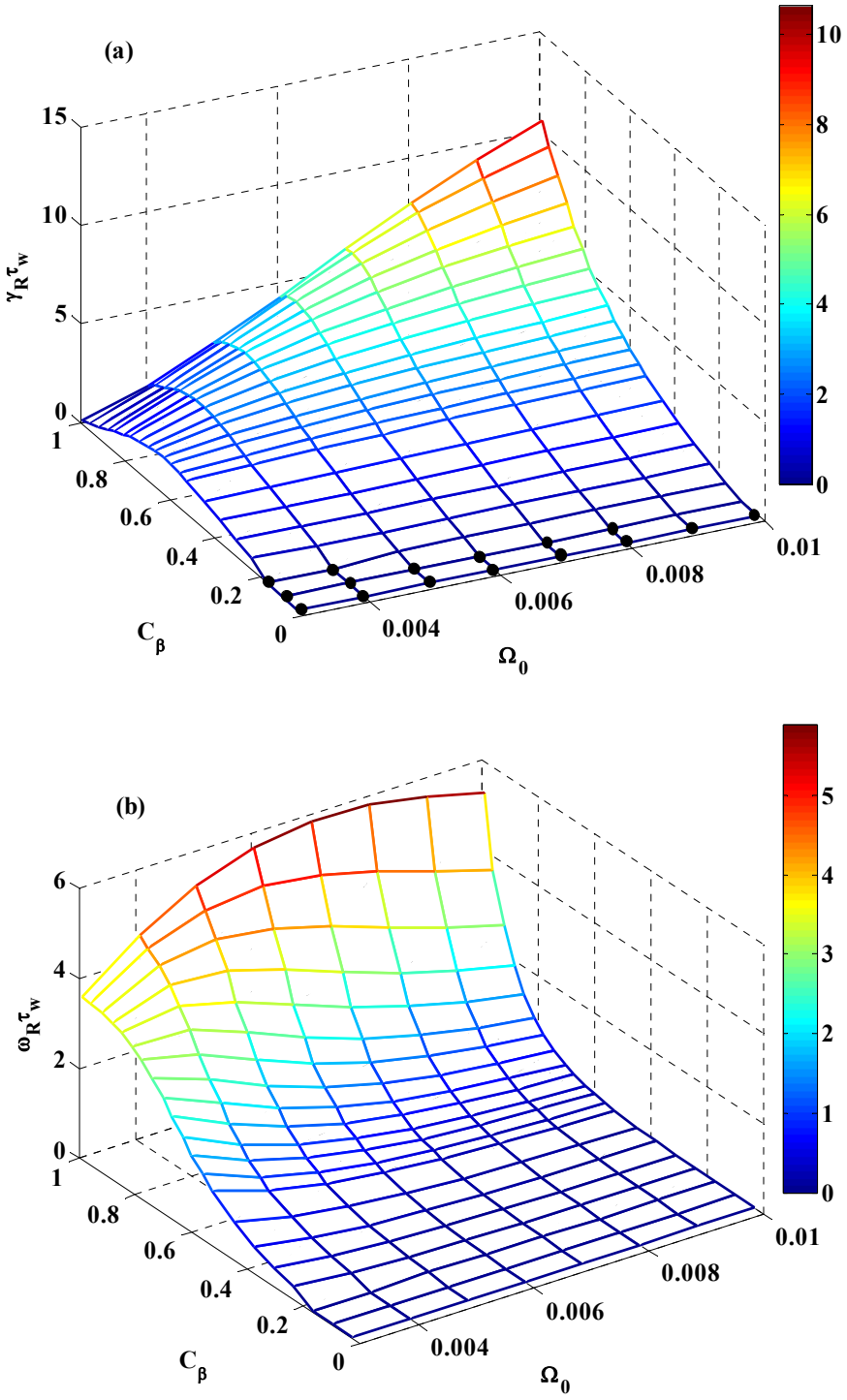

Figure 5. 2D plots of (a) growth rate and (b) mode frequency of the kinetic RWM, predicted by self-consistent kinetic computations with MARS-K. The parameters are $\eta = 0.0$, $\kappa_{\|} = 0.0$ and $d/a = 1.25$. Only precessional drift resonance damping of bulk plasma particles is included. The black dots indicate stable RWMs with practically vanishing growth rates.

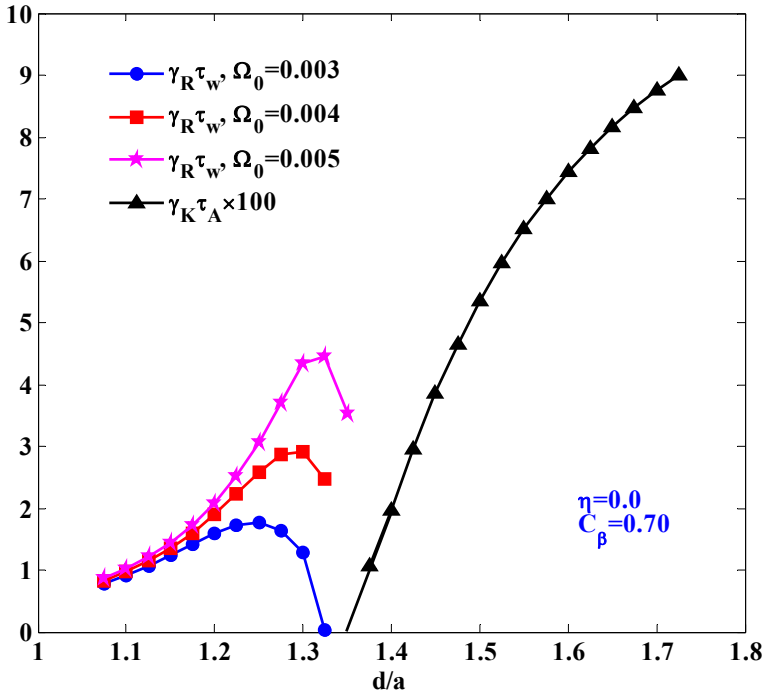

Figure 6. Growth rates of the RWM (γ_R) and the XK (γ_K) versus the normalized wall position d/a for different plasma rotation frequencies $\Omega_0 = 0.003$ (solid circles), $\Omega_0 = 0.004$ (solid squares) and $\Omega_0 = 0.005$ (solid stars), respectively. The other parameters are $\eta = 0.0$, $\kappa_{\|} = 0.0$ and $C_\beta = 0.70$. Only precessional resonance damping is included. Ω_0 is normalized by the Alfven frequency Ω_A .

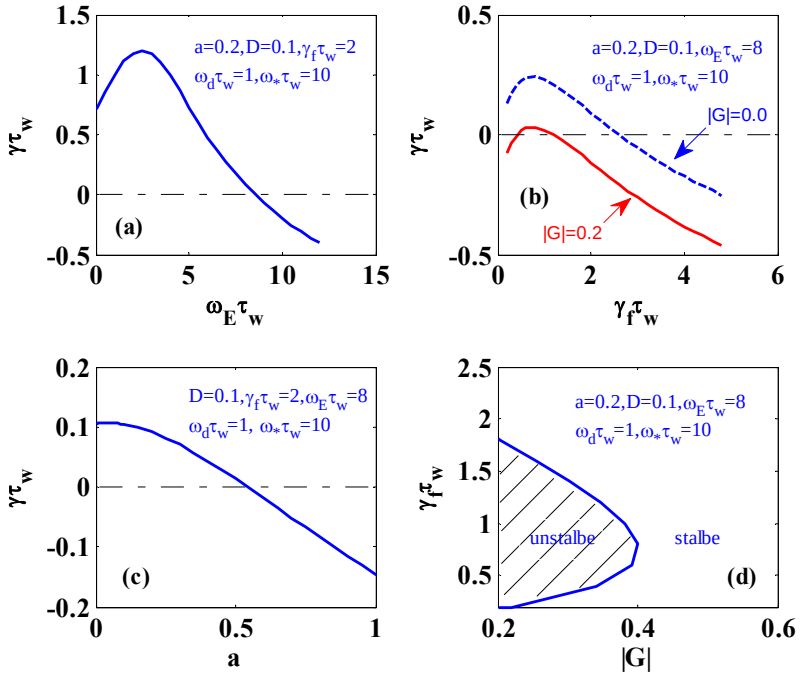

Figure 7. Summary of results obtained from a simple analytic model presented in Appendix A. (a) Growth rate of the kinetic RWM versus the $\mathbf{E}\times\mathbf{B}$ drift frequency. (b) Growth rate of the kinetic RWM versus the growth rate of the initial fluid RWM without the kinetic effects. The growth rate of the fluid RWM effectively represents the wall radial position. Compared are two cases: one with feedback, $|G|=0.2$ (solid line) and one without feedback $|G|=0.0$ (dashed line). (c) Growth rate of the kinetic RWM versus the parameter a (representing the kinetic contribution). (d) The stability boundary in the $|G|-\gamma_f\tau_w$ plane.

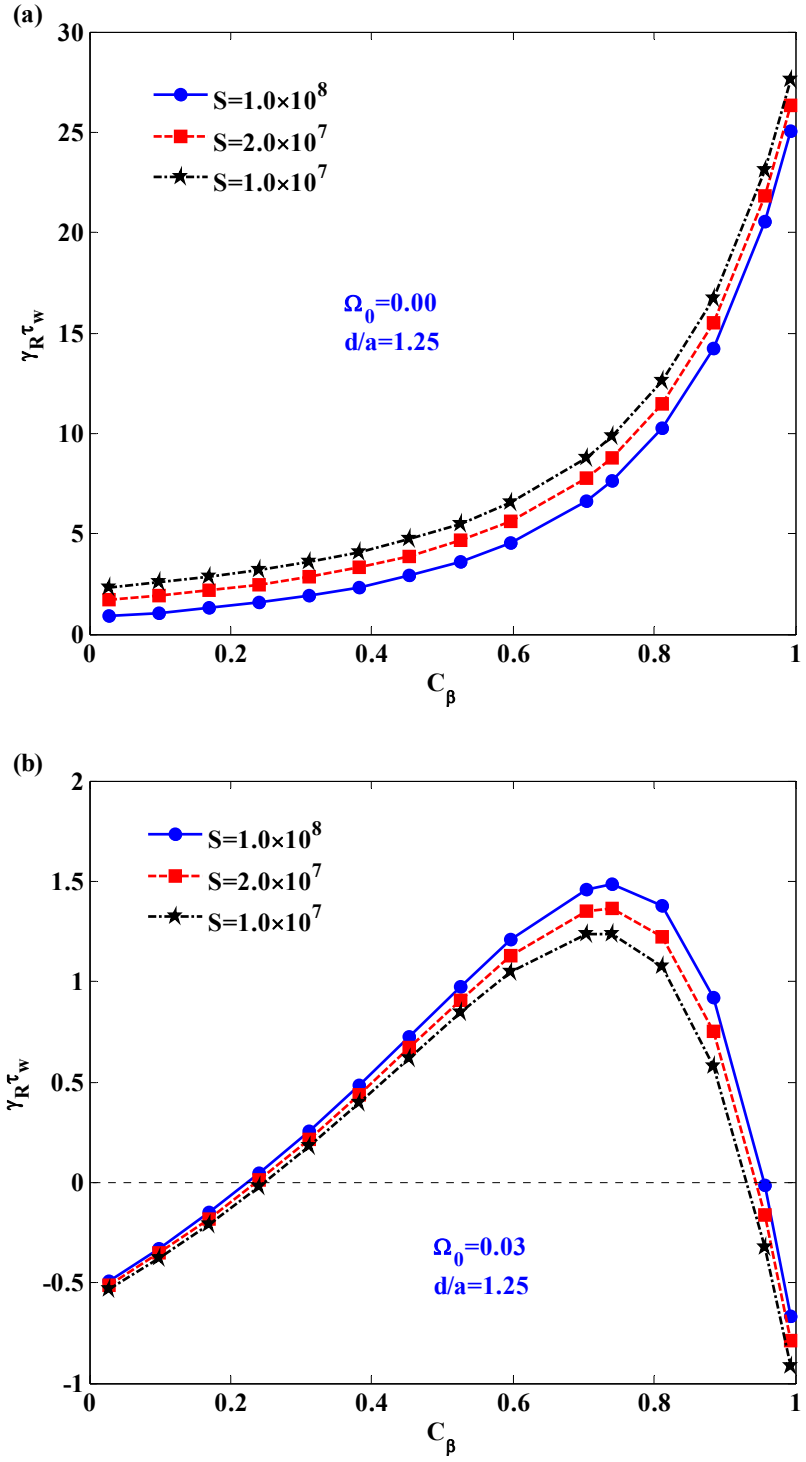

Figure 8. Growth rates of the fluid RWM versus C_β for different values of magnetic Lundquist number S: $S=1.0\times10^8$ (solid circles), $S=2.0\times10^7$ (solid squares) and $S=1.0\times10^7$ (solid stars), respectively, predicted by MARS-F at (a) vanishing plasma flow $\Omega_0=0.00$ and (b) $\Omega_0=0.03$. The other parameters are $\kappa_{||}=1.5$ and

$d/a = 1.25$.

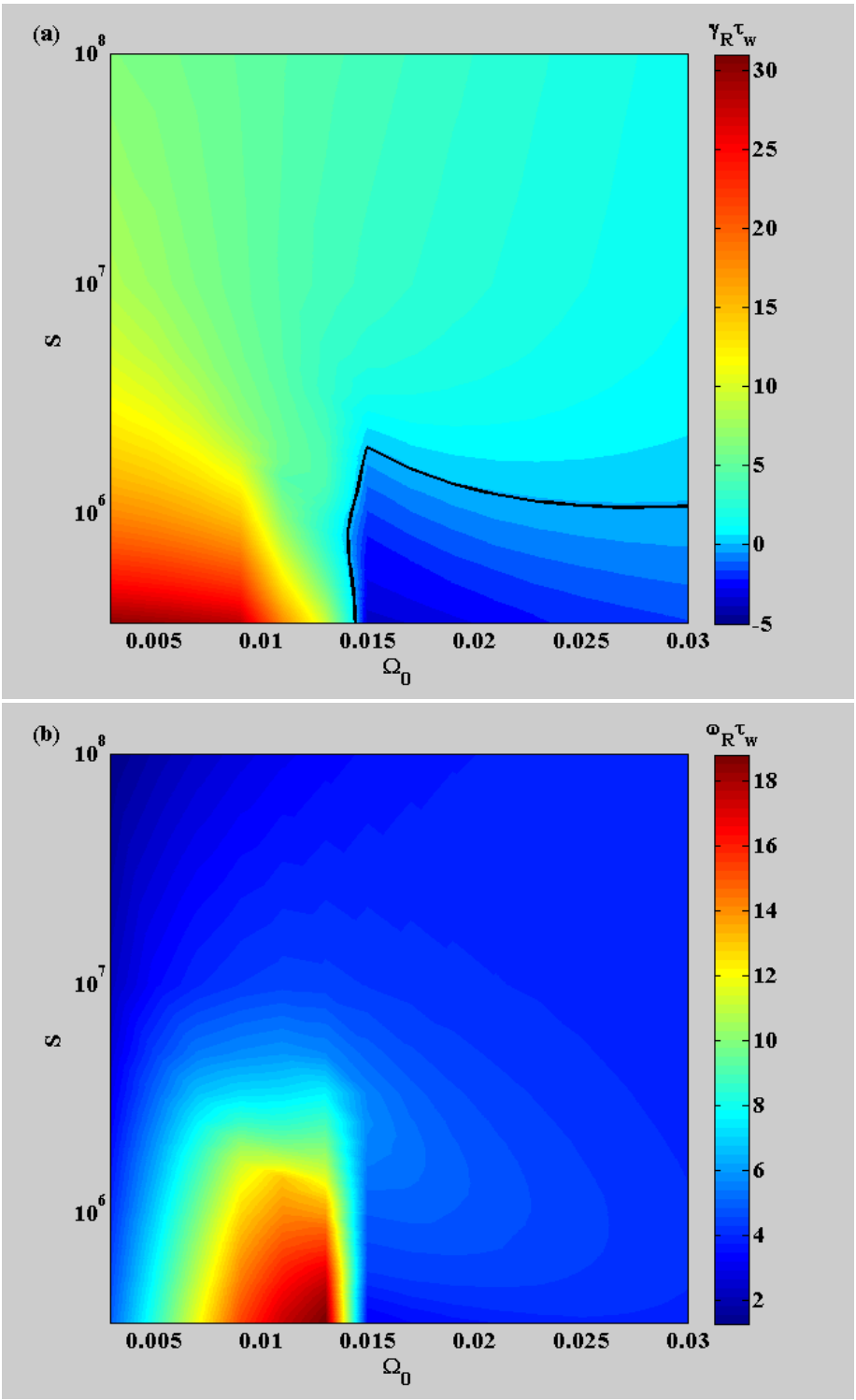

Figure 9. (a) Growth rate and (b) mode frequency of the fluid RWM with varying plasma rotation frequency Ω_0 and the magnetic Lundquist number S. The other

parameters are $\kappa_{\|} = 1.5$, $C_{\beta} = 0.70$ and $d/a = 1.25$. The solid curve shows the stability boundary in the $\Omega_0 - S$ plane.

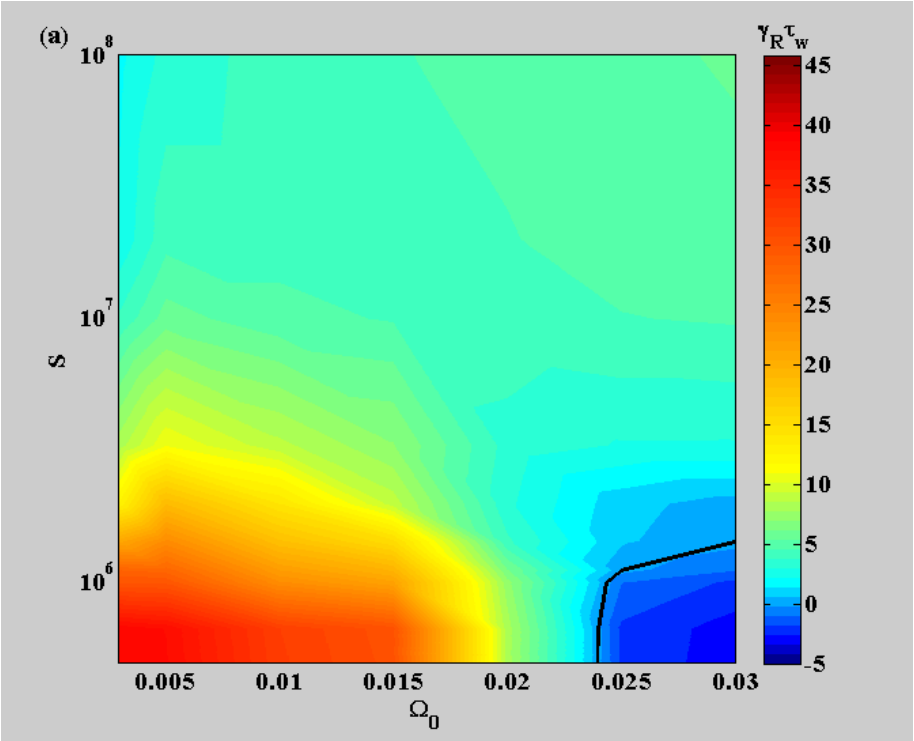

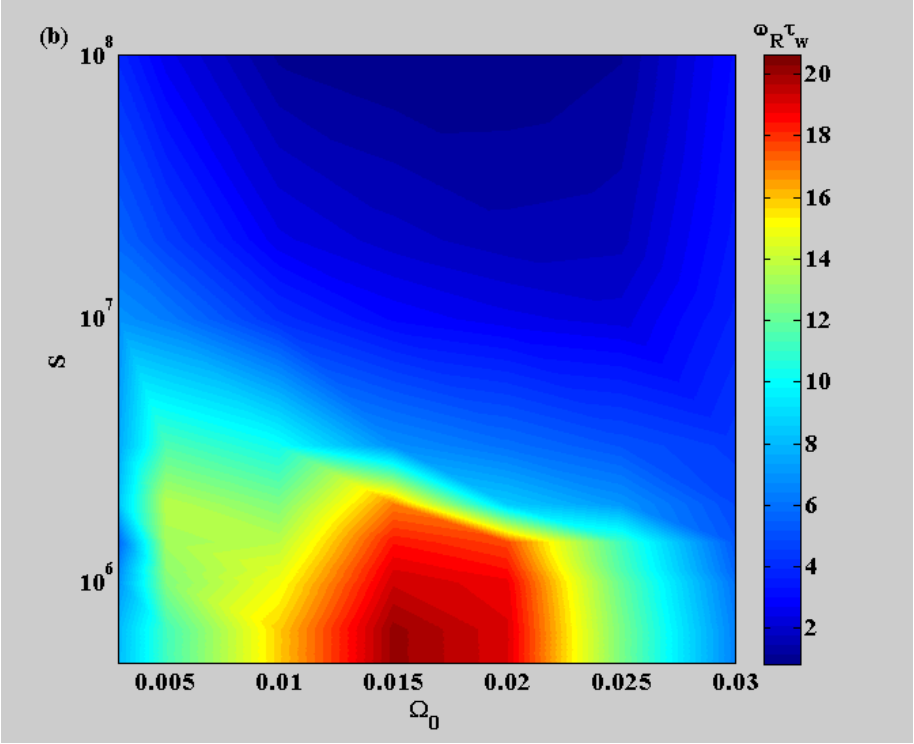

Figure 10. (a) Growth rate and (b) mode frequency of the kinetic RWM with varying plasma rotation frequency Ω_0 and the magnetic Lundquist number S, predicted by self-consistent kinetic computations with MARS-K. Only the precessional drift resonance damping of bulk plasma particles is included. The other parameters are $\kappa_{\|} = 0.0$, $C_\beta = 0.70$ and $d/a = 1.25$. The solid curve shows the stability boundary in the $\Omega_0 - S$ plane.

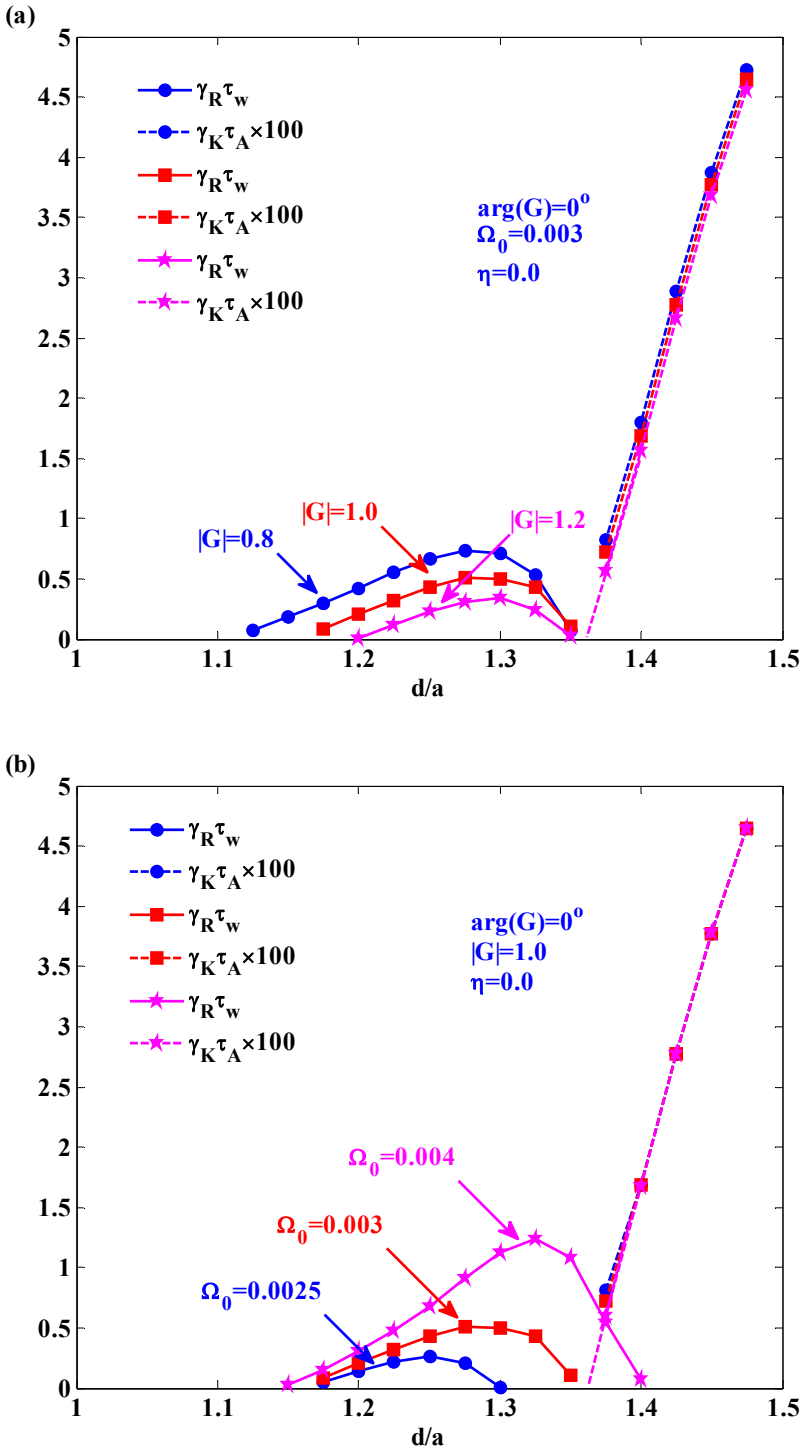

Figure 11. Growth rates of the kinetic RWM (γ_R) and the XK (γ_K) versus the normalized wall position d/a for (a) different values of the feedback gain, $|G|=0.8$ (solid circles), $|G|=1.0$ (solid squares) and $|G|=1.2$ (solid stars), at fixed rotation frequency $\Omega_0=0.003$, and (b) different rotation frequencies, $\Omega_0=0.0025$ (solid

circles), $\Omega_0 = 0.003$ (solid squares) and $\Omega_0 = 0.004$ (solid stars), at fixed feedback gain $|G| = 1.0$. The other parameters are $\kappa_{\|} = 0.0$, $C_\beta = 0.70$, $\arg(G) = 0^\circ$, and $\eta = 0.0$. The feedback gains are the same for the upper and the lower coils. Ω_0 is normalized by the Alfven frequency Ω_A and $|G|$ is normalized by $G_0 = R_0/\mu_0$. The poloidal sensor is used in the feedback logic.

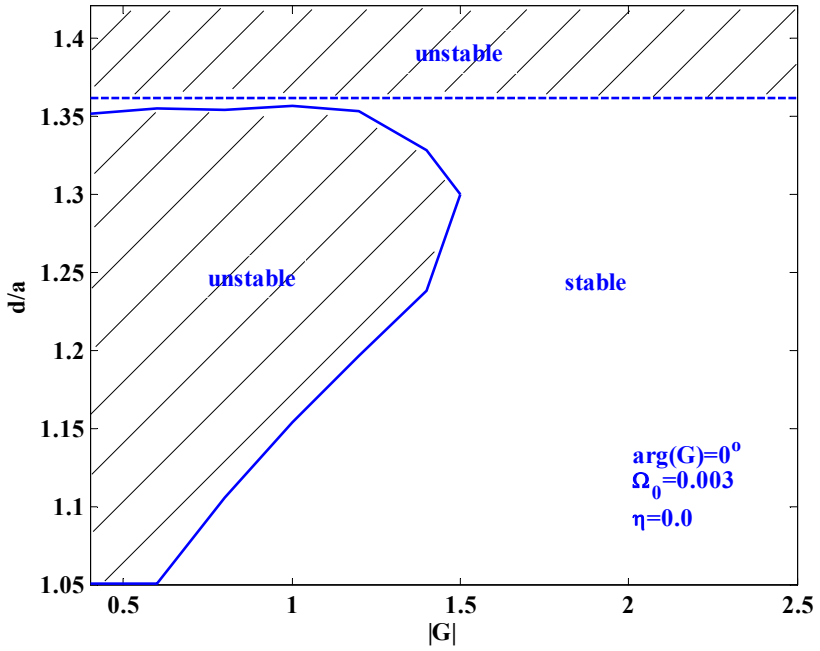

Figure 12. Stability boundary in the $|G| - d/a$ plane with the $b_\theta - sensor$, predicted by self-consistent kinetic computations with MARS-K. Only precessional drift resonance damping of bulk plasma particles is included. The other parameters are $\kappa_{\|} = 0.0$, $C_\beta = 0.70$, $\arg(G) = 0^\circ$, $\Omega_0 = 0.003$ and $\eta = 0.0$. The feedback gains for the upper and the lower coils are the same.

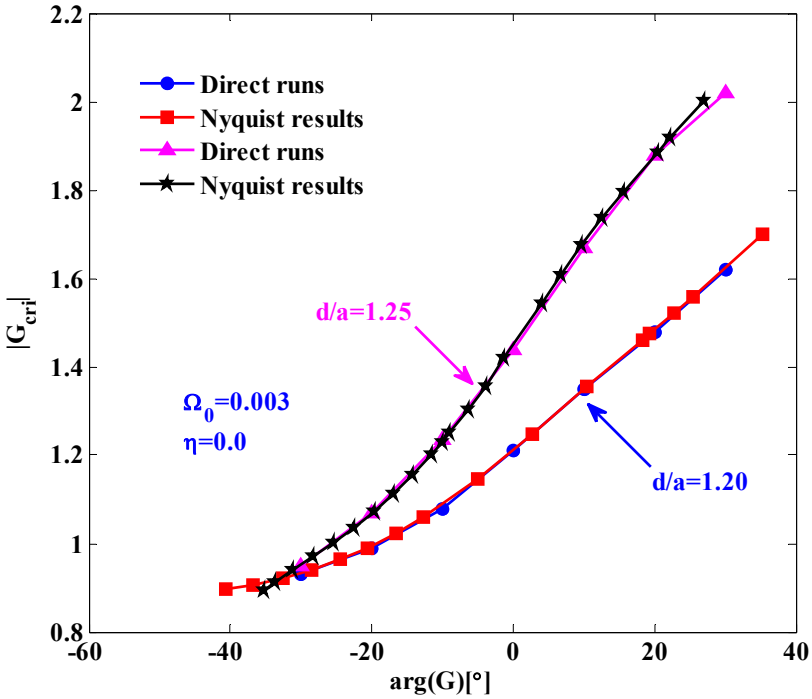

Figure 13. The critical gain amplitude versus the phase of the feedback gain, $\arg(G)$, for two choices of the wall position, $d/a=1.20$ (solid circles and solid squares) and $d/a=1.25$ (solid triangles and solid stars), respectively, as predicted by self-consistent kinetic runs. Compared are results from two different approaches – the direct feedback run and the Nyquist approach based on the open-loop response transfer function. The other parameters are $\kappa_{\|}=0.0$, $C_{\beta}=0.70$, $\Omega_0=0.003$ and $\eta=0.0$. The feedback gains are the same for the upper and lower coils, with the same poloidal sensor signal. Ω_0 is normalized by the Alfven frequency Ω_A and $|G_{\mathrm{cri}}|$ is normalized by $G_0=R_0/\mu_0$.

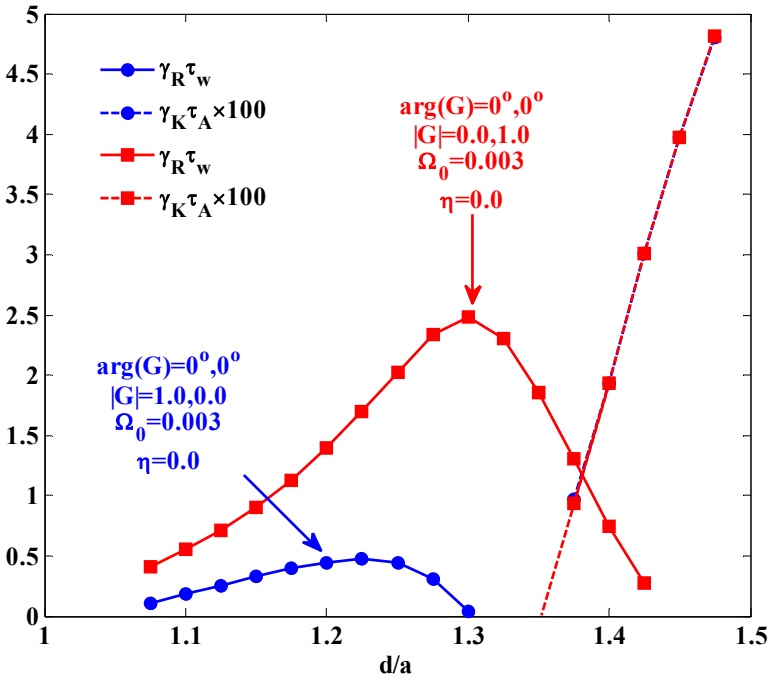

Figure 14. Growth rates of the kinetic RWM and the XK versus the wall position d/a, with only one feedback coil in action, $|G|=1.0,0.0$ (solid circles) and $|G|=0.0,1.0$ (solid squares), respectively, and with the $b_\theta-sensor$. The other parameters are $\kappa_{\|}=0.0$, $C_\beta=0.70$, $\arg(G)=0^\circ,0^\circ$, $\Omega_0=0.003$ and $\eta=0.0$.

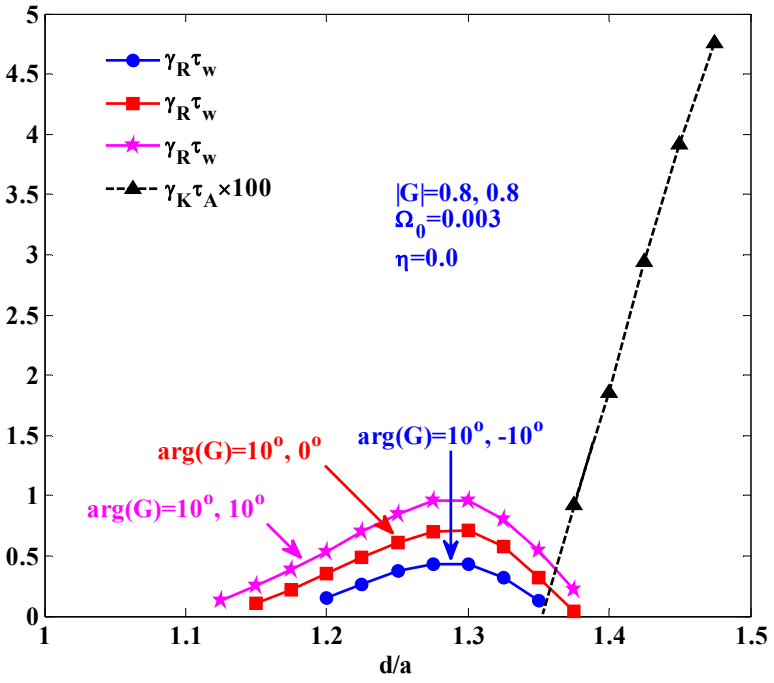

Figure 15. Growth rates of the kinetic RWM and the XK versus the wall position d/a, with different toroidal phases of feedback gain for the upper and lower coils, $\arg(G)=10^{\circ},-10^{\circ}$ (solid circles), $\arg(G)=10^{\circ},0^{\circ}$ (solid squares) and $\arg(G)=10^{\circ},10^{\circ}$ (solid stars). The other parameters are $\kappa_{\|}=0.0$, $C_{\beta}=0.70$, $|G|=0.8,0.8$, $\Omega_0=0.003$ and $\eta=0.0$.

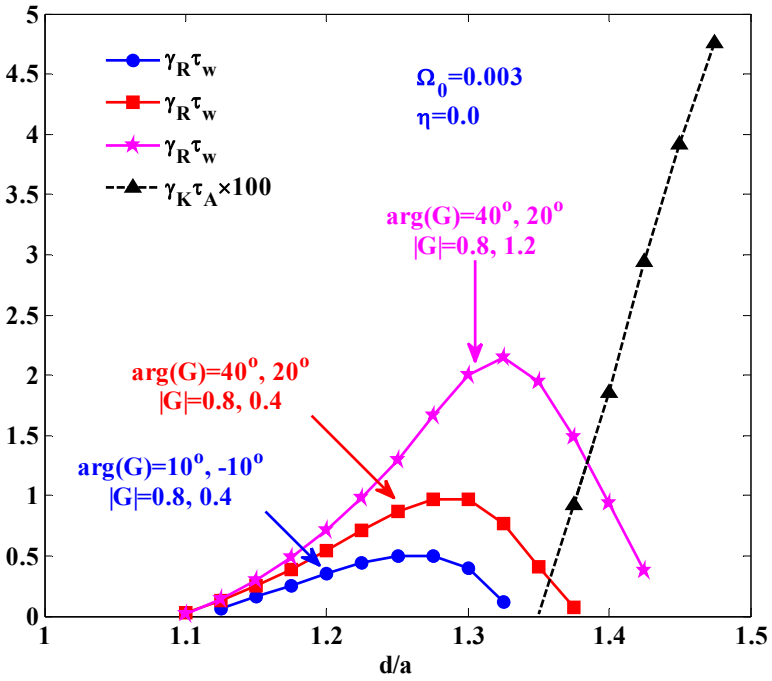

Figure 16. Growth rates of the kinetic RWM and the XK versus the wall position d/a, with varying both amplitude and phase of feedback gains between upper and lower coils, $\arg(G)=10^\circ,-10^\circ$, $|G|=0.8,0.4$ (solid circles), $\arg(G)=40^\circ,20^\circ$, $|G|=0.8,0.4$ (solid squares) and $\arg(G)=40^\circ,20^\circ$, $|G|=0.8,1.2$ (solid stars). The other parameters are $\kappa_{||}=0.0$, $C_\beta=0.70$, $\Omega_0=0.003$ and $\eta=0.0$.

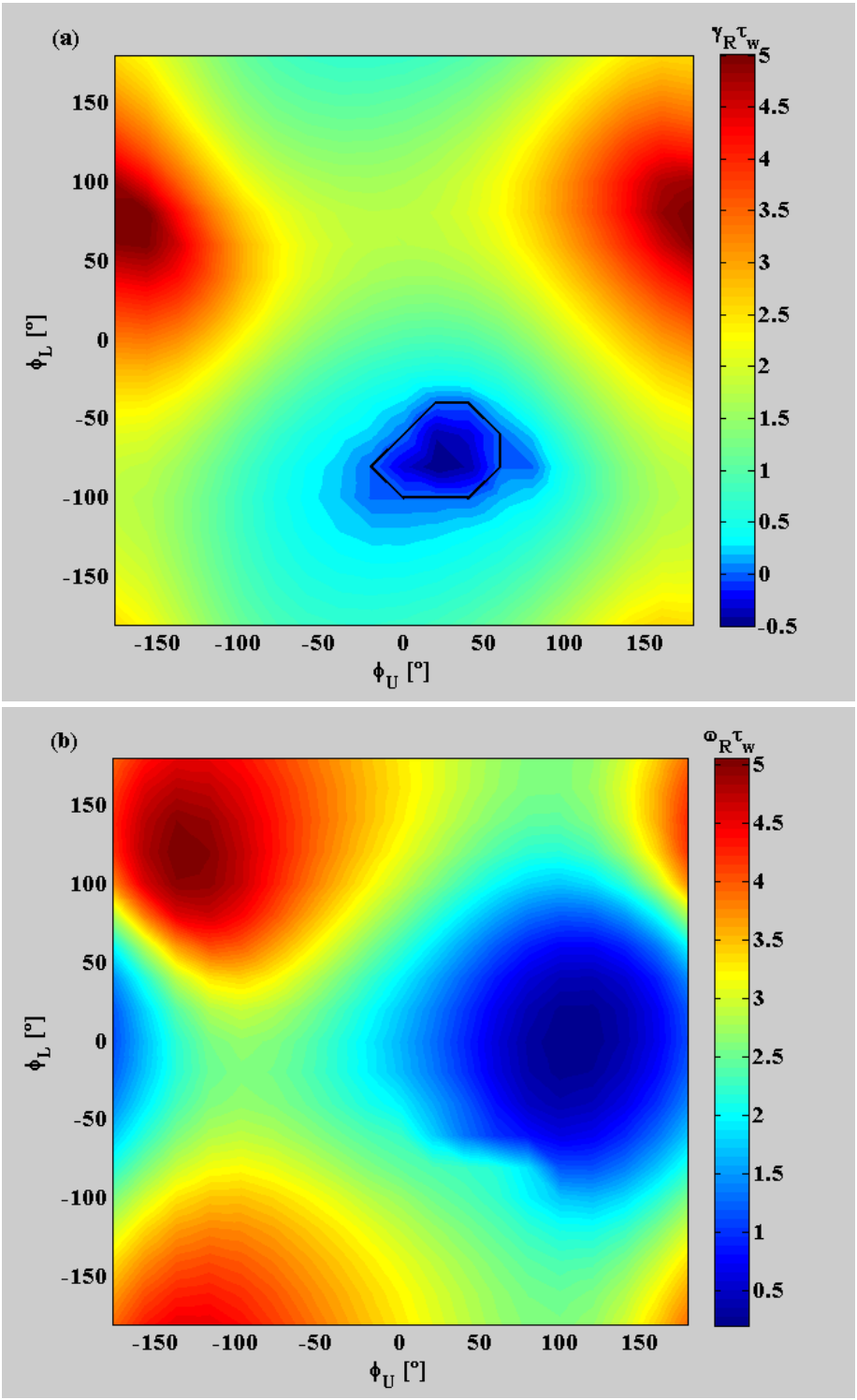

Figure 17. (a) Growth/damping rate and (b) mode frequency of the MARS-K computed kinetic RWM with varying phase of feedback gains for both the upper coil ϕ_U and lower coil ϕ_L. The other parameters are $\kappa_{\|} = 0.0$, $C_\beta = 0.70$, $|G| = 0.6, 0.6$, $\Omega_0 = 0.003$, $\eta = 0.0$ and $d/a = 1.25$. The solid curve shows the stability boundary

in the $\phi_U - \phi_L$ plane.

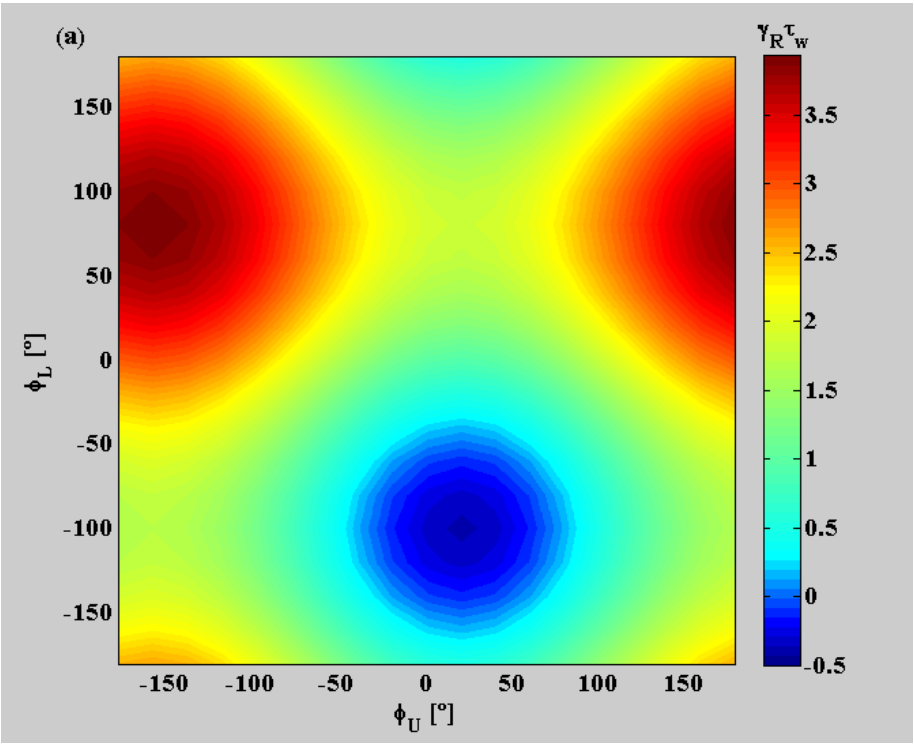

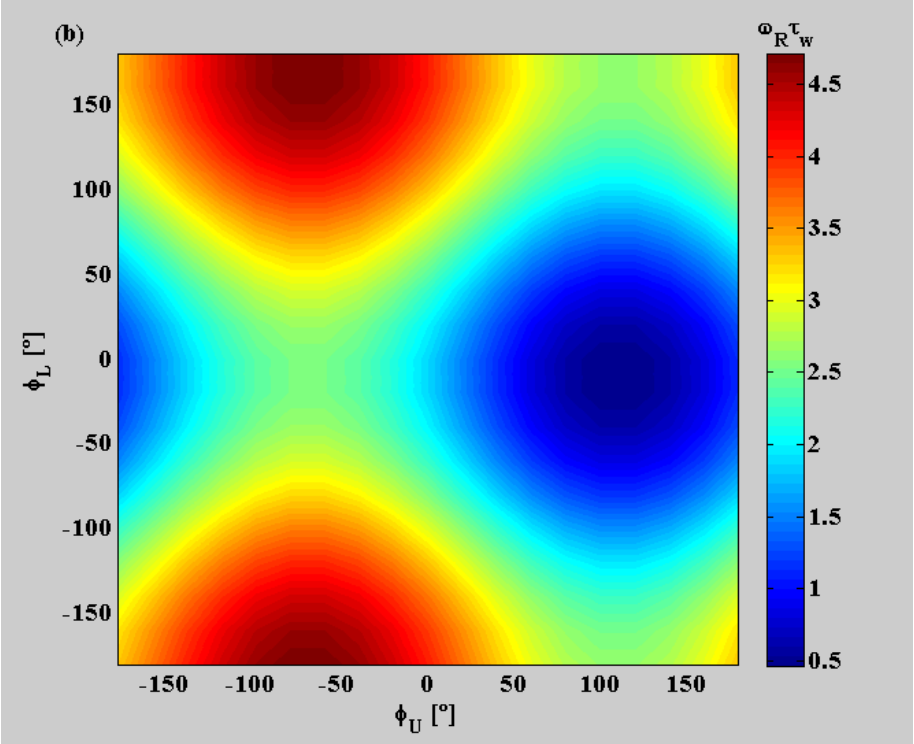

Figure 18. (a) Growth/damping rate and (b) mode frequency of the RWM from a single-pole analytic model, with varying feedback gain phase of the upper coil ϕ_U and the lower coil ϕ_L. The choices of parameters in the model, described in Appendix C, are $\gamma_0 = 1.77\times10^{-4}$, $\omega_0 = 2.59\times10^{-4}$, $|G| = 0.6$, $\hat{\phi}_U = -20^\circ$, $\hat{\phi}_L = 100^\circ$, $|R_U| = 1.75\times10^{-4}$, $|R_L| = 1.85\times10^{-4}$.